ELSEVIER

Thin Solid Films 365 (2000) 348–367

thin solid films

www.elsevier.com/locate/tsf

Modeling and simulation of plasma etching reactors for microelectronics

Demetre J. Economou

Plasma Processing Laboratory, Department of Chemical Engineering, University of Houston, Houston, TX 77204-4792, USA

Abstract

As microelectronic devices continue to shrink and process requirements become ever more stringent, plasma modeling and simulation becomes increasingly more attractive as a tool for design, control, and optimization of plasma reactors. A brief introduction and overview of the plasma reactor modeling and simulation problem is presented in this paper. The problem is broken down into smaller pieces (reactor, sheath, microfeature, and crystal lattice) to address the disparity in length scales. A modular approach also helps to resolve the issue of disparity in time scales. © 2000 Elsevier Science S.A. All rights reserved.

Keywords: Plasma etching reactor; Plasma modeling; Plasma simulation

1. Introduction

Low pressure (0.1 mTorr–10 Torr), cold (gas temperature 300–500 K), weakly ionized (degree of ionization 10^{-6}–10^{-1}) glow discharge plasmas are used extensively in the processing of electronic materials, especially for etching and deposition of thin films [1,2]. Such plasmas also find application in surface modification (e.g. hardening, corrosion resistance), lighting, and even environmental remediation [3]. Fig. 1 is a schematic of a plasma etch process carried out in a capacitively coupled reactor. The case of polysilicon etching in a chlorine plasma is shown as an example. The plasma is generated by applying radio frequency power between a pair of parallel plates in a low pressure chamber (Fig. 1a). The Cl_2 feedstock gas is attacked by plasma electrons to produce Cl radicals and Cl_2^+ ions. Radicals diffuse or are convected by gas flow towards the wafer where they adsorb on the surface. Ions accelerate in the sheath naturally occurring over the wafer, and bombard the wafer vertical to its surface (Fig. 1b). The combination of radical and ion bombardment produces $SiCl_4$ product which desorbs and is removed by the gas flow. It is this directional ion bombardment which promotes anisotropic etching of microscopic features (Fig. 1c), whereby the film etches much faster in the vertical as compared to the horizontal direction. At the atomic level, ion bombardment produces a modified surface layer in which the reactant (Cl) is mixed within the silicon lattice (Fig. 1d) to a depth depending on the ion energy (~tens of Å). The energy deposited by ions promotes the formation of products that are either sputtered away or desorb spontaneously in the gas phase. Fig. 1 also demonstrates the disparity in length scales encountered in plasma processing. The wafer will soon become 300 mm in diameter, so the reactor scale is of the order of tens of cm. The sheath thickness ranges from 0.1 to 10 mm depending on the Debye length and the voltage applied to the electrode. The feature size is rapidly moving below the sub-quarter-micron regime. Finally the lattice has to be described on the Å length scale.

Plasmas are also used for the low temperature deposition of thin solid films, for example amorphous hydrogenated silicon, diamond, and a host of other materials. In plasma deposition, radicals adsorb on the wafer surface where they react to deposit a thin film. The film microstructure and properties (e.g. density, stress) can be influenced by energetic ion bombardment. Since the fundamentals of plasma physics and chemistry are the same for both plasma etching and plasma-assisted chemical vapor deposition (PECVD), the latter will not be discussed here. A review of PECVD can be found in Ref. [4]. Plasma polymerization is covered by Yasuda [5].

The goals of any plasma etch process are to achieve high etch rate, uniformity, selectivity, controlled shape of the microscopic features etched into the film (anisotropy), and no radiation damage. High etch rate is desirable to increase the process throughput (wafers/h). However, etch rate must be balanced against uniformity, selectivity, and anisotropy. Uniformity refers to achieving the same etch characteristics (rate, wall profile, etc.) across the wafer which is scaling up to

PII: S0040-6090(99)01056-1

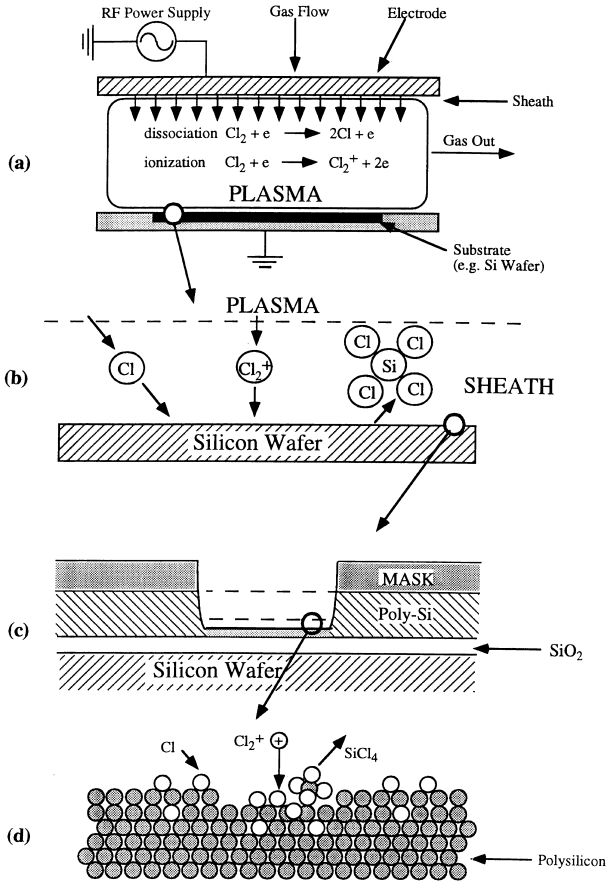

Fig. 1. Panorama of plasma etching using silicon etching with chlorine as an example. This figure also shows the disparate length scales involved from the reactor, to the sheath, to the microfeature, to the atomic scale. (a) Cl radicals and Cl_2^+ ions are generated in the plasma by electron impact of gas molecules. (b) Ions accelerate in the sheath and bombard the wafer along the vertical direction. (c) Ion bombardment induces anisotropic etching of microscopic features to yield $SiCl_4$, a volatile product. (d) Ion bombardment creates a modified layer at the surface where Cl is mixed within the Si lattice to a depth of tens of Å depending on the ion energy.

be 300 mm in diameter. Uniformity is necessary so that the underlying layer (silicon dioxide in Fig. 1c), for example, is not exposed to potentially harmful plasma radiation in some areas of the wafer while other areas are yet to clear of polysilicon. Also, plasma uniformity is needed to avoid nonuniform charging of the wafer which can lead to electrical damage. Selectivity refers to the relative rate of etching of one material with respect to another. Etch processes must be selective with respect to the mask and the underlying film. The mask must not be etched, otherwise the desired pattern will be distorted. Selectivity with respect to the underlying layer is particularly important when that layer is thin (gate oxide), or when the process uniformity is not good. The shape of the microscopic features etched into the wafer is of paramount importance. Often, anisotropic (vertical) sidewall profiles are required, perhaps with some roundness at the bottom of the feature. Radiation damage refers to structural damage of the crystal lattice or, more importantly, to electrical damage of sensitive devices caused by plasma radiation (ions, electrons, UV and soft X-ray photons) [6]. For example, spatially nonuniform current flowing from the plasma to the wafer can lead to charging and breakdown of thin oxides; or charging of insulating materials within a microfeature can lead to pattern distortion (notching), or high-energy ion bombardment can lead to structural damage of the top atomic layers of the etched film.

Choosing the reactor design and operating parameters are crucial for meeting the goals of plasma etching. There are many externally controlled variables (process inputs) which can influence the plasma characteristics, and in turn the process output (Fig. 2). Given a reactor type, its dimensions and materials of construction, one can manipulate operating parameters (pressure, power, frequency, etc.) to influence the process output (rate, uniformity, anisotropy, etc.). Plasma process development has been based largely on trial-and-error procedures guided by experience and intuition. As device dimensions continue to shrink and process requirements become more stringent, computer-aided design of plasma processes based on fundamental models becomes more attractive. A fundamental model is able to predict the key plasma properties bridging the input and output blocks as shown in Fig. 2.

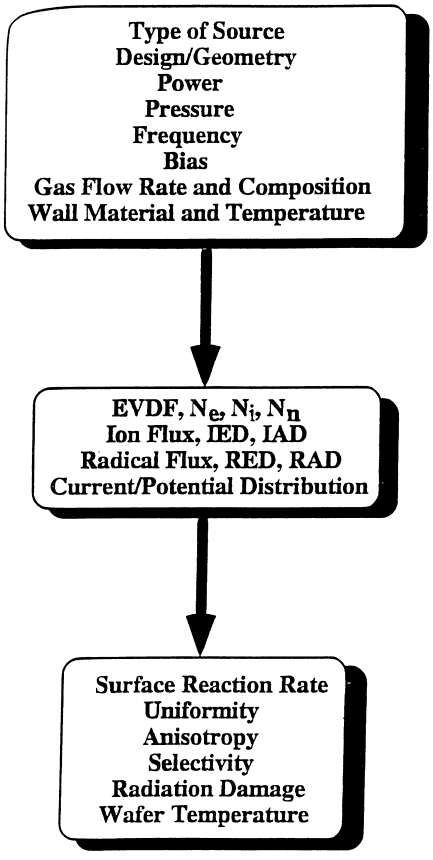

Fig. 2. Representation of the parameter space in plasma etching. The key internal plasma properties (middle) are the bridge between externally controlled variables (top) and the figures of merit (bottom).

Table 1
Typical parameter values for r.f. diode and high-density plasma (HDP) reactors [2]

Parameter	r.f. diode	HDP
Pressure (mTorr)	10–1000	0.5–50
Power (Watts)	50–2000	100–5000
Frequency (MHz)	0.05–13.56	1–2450
Volume (l)	1–10	1–50
Magnetic field (Gauss)	0–100	0–1000
Plasma density (cm^{-3})	10^9–10^{10}	10^{10}–10^{13}
Electron temperature (eV)	1–5	2–12
Heavy particle temperature (eV)	<0.1	<0.25
Ion bombardment energy (eV)	100–1000	20–300
Fractional ionization	10^{-6}–10^{-3}	10^{-4}–10^{-1}

2. Physical characteristics of plasmas

Plasmas used in electronic materials processing are low pressure glow discharges with operational and physical characteristics summarized in Table 1. These plasmas are strongly nonequilibrium systems. Electrons achieve very high temperatures (10,000s K) and are able to initiate and sustain plasma chemistry in a rather cold background gas (~400–500 K). Formation of a sheath is of critical importance to plasma processing. The strong sheath electric field (normally 100 times stronger than that in the bulk plasma) is pointing such that positive ions are accelerated towards the wall (Fig. 1b). Since the sheath thickness is much smaller than the lateral dimensions of the electrode, the electric field in the sheath is perpendicular to the macroscopic wafer surface. Hence ions acquire directional energy in the sheath and bombard the wafer along the surface normal. That way, horizontal surfaces which are exposed to ion bombardment etch much faster than vertical surfaces, resulting in anisotropic (vertical) etching. Low temperature processing and anisotropy are the most important attributes of plasma etching from the technological point of view. The sheath is further examined in Section 5.3.

The potential distribution in the reactor is such that the plasma potential is greater than any wall potential. Of importance to plasma processing is the difference between the plasma potential and the wall potential, namely, the sheath potential accelerating positive ions. In capacitively-coupled asymmetric systems (unequal electrode areas), a larger sheath potential develops over the smaller area electrode. In fact, the ratio of sheath potentials over the two electrodes of a diode having areas A_1 and A_2 is

$$\frac{V_1}{V_2} = \left(\frac{A_2}{A_1}\right)^n \quad (1)$$

Simple capacitive voltage division models predict an exponent $n = 4$ [2], but a value of $n \approx 1$–2 has been determined experimentally [7].

Fig. 3 shows the range of kinetic energies and densities of particles typically present in plasma processing reactors [8]. The nonequilibrium nature of the discharge is evident from the fact that different species have different energies. Ions bombarding the cathode (box C) and the secondary electrons (box A) they emit (which stream back into the plasma) have the highest energies since they are accelerated through a high-voltage sheath. Ions in the bulk plasma (box F) are only accelerated by the much weaker bulk fields and have much lower energies (and temperatures). Neutral species (feedstock gas and reaction products) are orders of magnitude more abundant than charged species and have much lower (thermal) energies (box G). There can be a significant concentration of neutrals (and ions) that are 'hot' (Box E). These result from dissociation or dissociative ionization reactions where the excess electron energy is deposited as kinetic energy of the product fragments. At low pressures, these fragments do not suffer enough collisions to thermalize [9]. In plasmas of interest the velocity of electrons is much higher than that of positive ions which in turn is much higher than that of neutrals. In addition, electrons have a nearly isotropic velocity distribution, while positive ions have very anisotropic velocity distribution (directed along the electric field). The ordering of electron, ion, and neutral gas temperatures is $T_e >> T_i \sim T_g$.

3. Plasma chemistry

3.1. Gas-phase chemistry

Several steps are typically involved in plasma etching. Radicals generated in the plasma by electron impact dissociation of gas molecules (step 1) diffuse or are convected by gas flow to the surface (step 2) where they adsorb (step 3). The adsorbed species (adspecies) react with the surface to form products (step 4). The products then desorb (step 5) and diffuse back into the gas phase (step 6). The surface

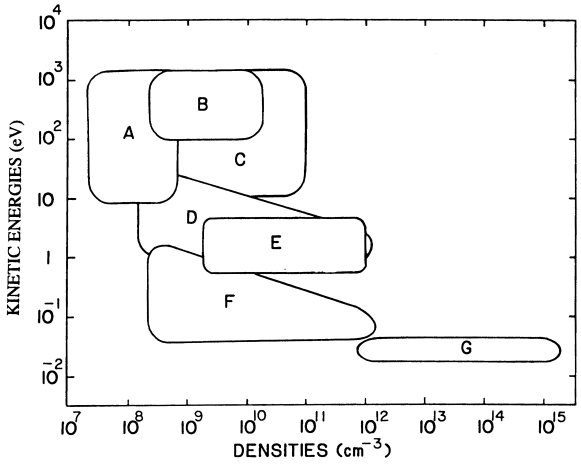

Fig. 3. Range of kinetic energies and densities of species typically present in glow discharge plasmas. A, secondary electrons accelerated through the sheath; B, ions backscattered from cathode (most likely neutralized); C, ions accelerated towards cathode; D, electrons in bulk plasma; E, hot ions and neutrals formed in dissociation reactions (Frank–Condon effect); F, ions in bulk plasma; G, neutral atoms and molecules. After Ref. [8].

processes may be strongly influenced by energetic particle bombardment of the surface, including positive ions, electrons and photons. Of these, positive ion bombardment is thought to be most important. Negative ions are excluded because they are not energetic enough to overcome the sheath potential barrier and reach the wafer. It must be emphasized that product volatility is a necessary condition for etching to occur. Otherwise, the products block the surface and the reaction stops altogether.

Plasma chemistry starts with electron impact reactions. The corresponding reaction rate is given by [2,10]

$$R_{ei} = n_e n_i \langle v\sigma(v)\rangle = n_e n_i \int v\sigma(v) f(\boldsymbol{v},\boldsymbol{r},t)\mathrm{d}\boldsymbol{v} \quad (2)$$

where the average $\langle\sigma(v)v\rangle$ is taken over the electron velocity distribution function (EVDF) $f(\boldsymbol{v},\boldsymbol{r},t)$. Here n_e and n_i are the number density of the electrons and the collision partner, respectively, $\boldsymbol{v}$ and $\boldsymbol{r}$ are the electron velocity and position vectors, respectively, v is the magnitude of the velocity vector (speed), and $\sigma(v)$ is the collision cross section, which is a measure of the 'effectiveness' of the particular interaction between an electron and a neutral. Determination of the distribution function is one of the central problems in understanding plasma chemistry. The EVDF is defined in the phase-space element $\mathrm{d}\boldsymbol{v}\mathrm{d}\boldsymbol{r}$ such that $f(\boldsymbol{r},\boldsymbol{v},t)\mathrm{d}\boldsymbol{v}\mathrm{d}\boldsymbol{r}$ is the number of electrons $\mathrm{d}n_e$ at time t located between $\boldsymbol{r}$ and $\boldsymbol{r}+\mathrm{d}\boldsymbol{r}$ which have velocities between $\boldsymbol{v}$ and $\boldsymbol{v}+\mathrm{d}\boldsymbol{v}$. When normalized by the total number of electrons n_e, it is a probability density function. The EVDF is obtained by solving the Boltzmann transport equation [11,12]

$$\frac{\partial f(\boldsymbol{r},\boldsymbol{v},t)}{\partial t} + \boldsymbol{v}\cdot\frac{\partial}{\partial \boldsymbol{r}} f(\boldsymbol{r},\boldsymbol{v},t) + \frac{\boldsymbol{F}}{m_e}\cdot\frac{\partial}{\partial \boldsymbol{v}} f(\boldsymbol{r},\boldsymbol{v},t) = \left(\frac{\partial f(\boldsymbol{r},\boldsymbol{v},t)}{\partial t}\right)_{col} \quad (3)$$

The right-hand side of Eq. (3) is the so-called collision integral which accounts for changes of the EVDF because of collisions electrons undergo mainly with neutrals but also with other electrons and ions. $\boldsymbol{F} = e(\boldsymbol{E} + \boldsymbol{v}\times\boldsymbol{B})$ is the Lorenz force acting on the electrons, where $\boldsymbol{E}$ and $\boldsymbol{B}$ are the electric field and magnetic induction, respectively, and m_e is the electron mass. Eq. (3) is a partial integro-differential equation in seven dimensions (three in space, three in velocity and time), and as such is extremely difficult to solve. In the expressions above, $\boldsymbol{v}$ is the individual particle velocity not to be confused with the average velocity of the ensemble of particles.

Meeks and Ho [13] discuss a methodology for formulating gas-phase and surface chemistry mechanisms relevant to plasma reactor simulations. References to sources for chemistry and transport data are also found in their paper.

3.2. Surface chemistry

Surface reactions are of ultimate importance since the goal of plasma processing is surface modification. One can distinguish between several types of processes [14] which can occur on the surface of a solid exposed to a plasma. The surface is bombarded by neutral radicals and molecules, positive ions, electrons, and photons. Of these, neutral specie and positive ion bombardment is generally considered most important. Sputtering refers to the process of ejection of surface atoms induced by ions transferring momentum to the surface [15]. Sputtering can be thought of as atomic scale sandblasting. This is a physical rather than a chemical mechanism, and as such has very low selectivity. For ion energies of interest, the etch rate due to sputtering is given by [16]

$$\mathrm{ER}_s = Y_s\frac{J_+}{\rho_s} = \alpha(\varepsilon_+^x - \varepsilon_{th}^x)\frac{J_+}{\rho_s} \quad (4)$$

where $x = 0.5$, Y_s is the sputtering yield (atoms of substrate removed per incident ion), J_+ and ε_+ are the ion flux and energy, respectively, and ρ_s is the density of the substrate material; α is a constant characteristic of the material, and ε_{th} is the sputtering threshold. The latter is the minimum ion energy required for sputtering to occur at all. Plasma etching systems are designed to minimize sputtering. Ion bombardment can also result is ejection of electrons (secondary electrons) from the surface. The secondary electron emission yield (electrons per incident ion) depends mainly on the type of surface and the ion energy [15].

In chemical etching neutrals react with the surface spontaneously to yield product. An example is etching of silicon with F atoms, $\mathrm{Si} + 4\mathrm{F} \rightarrow \mathrm{SiF_4}$. Rapid surface fluorination leads to $\mathrm{SiF_4}$ which desorbs into the gas. Ion bombardment is not necessary for this reaction to occur. Generally, chemical etching has very high selectivity. Instead of etching, radicals can recombine on the surface. This may be an important loss mechanism of potential etchant species, especially at low pressures. Ion bombardment can influence one or more of the surface reaction steps in plasma etching. For example, ion bombardment disrupts the crystal lattice generating 'active' sites where neutrals can adsorb (step 3 above), or ions promote the reaction of adsorbed species with the substrate (step 4), or ions clear the surface from adsorbed products (by sputtering) thereby exposing 'fresh' surface to the incoming etchant flux. In ion-induced etching, reaction between a species and the substrate occurs only in the presence of ion bombardment. An example is etching of undoped silicon with chlorine. At the molecular level, ion bombardment induces mixing of the adsorbed gas (Cl) with the crystal by the so-called collision cascade [17]. The depth of the mixed layer depends on the ion energy, and typically extends some tens of Å into the crystal lattice. Energy deposited by the ions in the mixed layer favors the formation of weakly bound species (SiCl_x) that are either sputtered away or desorb spontaneously into the gas phase. The formation of a surface layer is discussed further below (Section 5.5). In ion-enhanced etching, ion bombardment accelerates the reaction of etchant species with the substrate.

Without ion bombardment that reaction would still occur but at much reduced rate.

In general, the total etch rate can be expressed as the sum of three components: physical sputtering, spontaneous (chemical) etching and ion-induced or ion-enhanced etching [18,19].

$$ER_{tot} = ER_s + ER_c + ER_+ \quad (5)$$

All three processes can occur simultaneously when a surface is exposed to a plasma. The relative importance of one mechanism over the others depends on the material system (substrate and gas), the ratio of neutral to ion flux, and the ion energy. In general, conditions are selected such that ion assisted chemistry dominates. In cases that chemical etching dominates, a mechanism for wall passivation is necessary to avoid mask undercut.

In some cases ion bombardment has little or no effect on etching. A notable example is etching of aluminum in chlorine containing plasmas [20]. The etch rate is practically independent of ion energy; the only function of the ions in this case is to keep the surface 'clean' by sputtering away any adsorbates (e.g. oxygen forming aluminum oxide) that can potentially block etching. In still another situation, ion bombardment can retard etching as in the case of copper etching by chlorine [21].

4. Plasma reactors

4.1. Low-density plasma reactors

These have the operational characteristics shown under the 'r.f. diode' column of Table 1. An example of a low plasma density system is the capacitively-coupled diode shown in Fig. 1a. The substrate electrode can be made larger to hold many wafers, but due to the tendency of increasing wafer size, single wafer tools (processing one wafer at a time) are favored for improved uniformity and better process control. Fig. 1a shows a symmetric configuration (electrodes of equal area), that is normally operated at relatively high pressures (>100 mTorr); this is the so-called plasma etching configuration. As a result of collisions in the sheath, the energy of ions bombarding the wafer is rather low (<100 eV). A common variant of this diode consists of a substrate electrode and the chamber wall (grounded) as the counterelectrode. This is a strongly asymmetric system (1arge difference in electrode areas). As a result the sheath over the smaller (substrate) electrode attains a larger voltage (Eq. (1)). In addition, the operating pressures are relatively low (<100 mTorr) resulting in intense ion bombardment. This is referred to as reactive ion etching (RIE) or reactive sputter etching configuration. The addition of a magnetic field parallel to the wafer holder reduces electron losses and hence enhances the plasma density. At the same time the sheath potential is reduced minimizing unwanted sputtering. The resulting configuration is called magnetically enhanced reactive ion etching (MERIE) [1]. Oftentimes, the magnetic field is rotated to improve etch uniformity. In another variant of the diode reactor (so called triode) a third electrode is added to partially decouple plasma density and ion bombardment energy.

Volume-loaded barrel reactors [22] are not used for applications that require anisotropic etching. A typical example is photoresist stripping. High throughput is one of the advantages of the volume-loaded tools. The plasma is generated in the annular space between a quartz barrel and a concentric perforated metal cylinder (etch tunnel). The wafers are loaded on a quartz boat which is placed inside the etch tunnel. Reactive radicals formed in the plasma diffuse through the perforations of the etch tunnel and then diffuse in-between the wafers where they react [23]. When the plasma is confined in the annular space outside the tunnel, the wafers are not subjected to ion bombardment, but the wafers can still be exposed to plasma radiation. There are applications that require the wafers to be far away from the plasma so as to avoid electrical damage of devices built onto the wafers. In such cases a downstream etching reactor is used [24]. The plasma is generated at a remote location. Reactive radicals formed in the plasma are transported by gas flow downstream to the wafer chamber where etching occurs. If the plasma is far enough from the substrate, charged particles recombine before reaching the wafer. Thus the wafer is exposed to neutral species alone. This configuration is used only for applications that do not require anisotropic etching; for example, photoresist stripping and selective nitride etching over oxide.

4.2. High-density plasma (HDP) reactors

A disadvantage of the diode capacitively-coupled reactor (CCP) reactor is that the plasma (electron and ion) density cannot be controlled independently of the ion bombardment energy. As the applied r.f. voltage amplitude is increased to increase the plasma density, so does the sheath potential and consequently the ion bombardment energy. Excessive ion energy is not beneficial as it can lead to unwanted sputtering and heating of the wafer. Furthermore, etching of modern sub-quarter-micron device structures requires extreme directionality of the impinging ions. This can only be achieved by avoiding ion collisions in the sheath. Finally, etching of wafers with ever increasing diameter demands a uniform plasma over large areas. In an effort to satisfy these requirements, high (charge) density, low (gas) pressure plasmas have been developed [2]. Typical characteristics of these high-density plasmas (HDP) compared to conventional r.f. diodes are shown in Table 1. Salient features of HDP reactors are: (a) (quasi) independent control of plasma density and ion bombardment energy can be achieved by decoupling plasma generation from substrate (wafer) bias, (b) high plasma density (small Debye length) and low gas pressure (long mean free path) result in collisionless sheath that promotes ion directionality, and (c) low gas pressure

facilitates diffusion, promoting uniformity over large diameter substrates. Examples of HDP are inductively coupled plasma (ICP), helical resonator, electron cyclotron resonance (ECR), and helicon plasmas [25]. A common feature of these reactors is the separate zones for plasma production and wafer placement. These two zones can be tens of cm apart. Plasma is generated in the upper zone and diffuses into the lower part of the chamber enclosing the substrate. A set of optional multipole permanent magnets can surround the substrate chamber to minimize plasma losses to the walls, thus improving plasma density and also plasma uniformity.

Inductively coupled plasma (ICP) reactors (Fig. 4) are particularly attractive because their design is relatively simpler and they are scaleable to large diameter substrates [26]. In ICPs, the plasma is excited in a cylindrical chamber (r, z, θ) by a helical (solenoidal) or planar (stovetop-type) coil powered at radio frequencies, for example 13.56 MHz. The coil current induces a time-varying magnetic field which in turn induces an azimuthal (in the θ-direction) electric field that couples power to the plasma, i.e. heats the plasma electrons. For common excitation frequencies (less than the plasma frequency), the electromagnetic fields are absorbed by the plasma within the skin depth. For typical conditions, fields penetrate a few cm into the plasma. The power is deposited nonuniformly in the shape of a toroid (see Fig. 8 below). Because of the low pressure, however, species diffusion is facile and the plasma fills the whole reactor. In the absence of any capacitive coupling from the coil, the plasma potential is relatively low (~20 V) thus minimizing unwanted sputtering of the reactor walls. Capacitive coupling from the coil can result in larger plasma potentials. The wafer platen can be biased independently by a separate r.f. power supply in order to control the energy of ions bombarding the wafer. As in the case of capacitive coupling from the coil, larger (but controllable) time-dependent plasma potentials are then established.

5. Plasma modeling and simulation

Modeling and simulation of plasma systems has emerged as a tool for enhancing one's intuition about the physicochemical processes occurring in the plasma, for understanding the complex spatiotemporal plasma dynamics, and for assisting in the design of new reactors or the optimization of existing ones [27,28]. The problem can be summarized by Fig. 2. Given a reactor type and configuration, geometrical dimensions and materials of construction, as well as a set of operating parameters (inputs including plasma power, gas pressure, excitation frequency, substrate voltage or power, and feedstock gas composition and flow rate), determine the following key plasma properties: The electron velocity distribution function (EVDF), the space and time variation of electron, ion, and neutral species densities and velocities, the flux, energy and angular distribution of ions and neutrals bombarding the electrodes and their uniformity across the electrodes, and the potential and current distribution in the

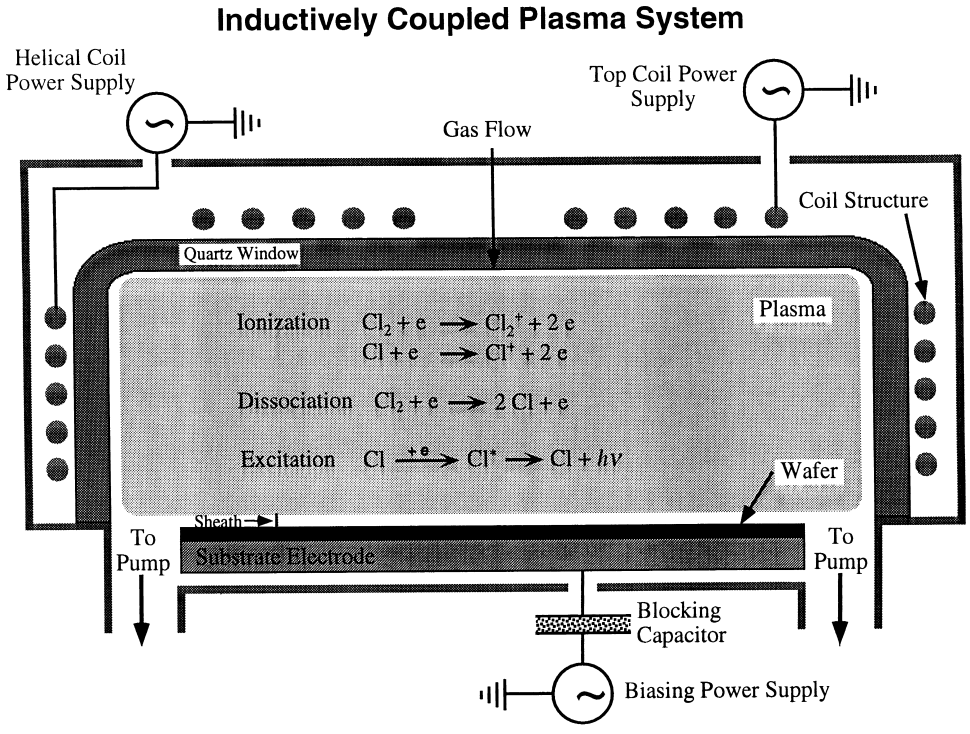

Fig. 4. Schematic of an inductively coupled plasma reactor. The reactor can have a helical (solenoidal) coil and/or a planar (stove-top) coil. The substrate electrode can be biased independently to adjust the energy of ions bombarding the wafer.

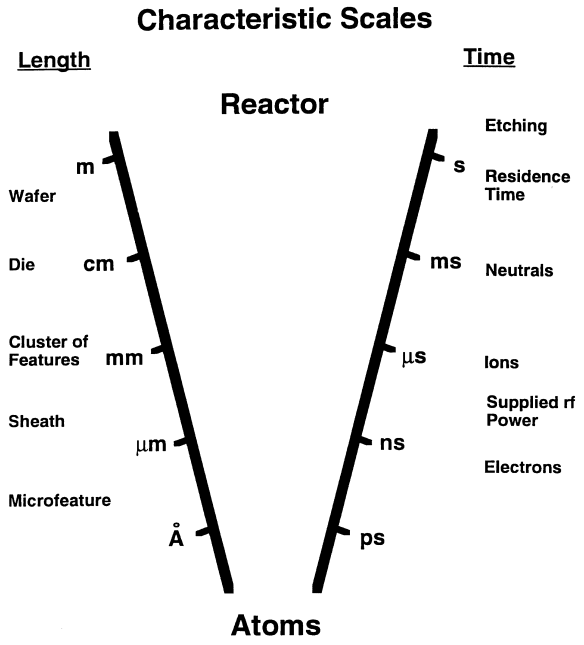

Fig. 5. Disparity in length and time scales in plasma processing. From atoms to reactor.

system. These variables and their spatiotemporal variation provide insight into the plasma reactor behavior. When the reactor is loaded with a wafer, one is in addition interested in the outputs (figures of merit) including the etch (or deposition) rate, uniformity, anisotropy, selectivity, radiation damage, and wafer temperature. One can also pose the inverse problem which is much more difficult to solve, that is: given a material to be etched (or deposited) and specifications on the rate, uniformity, anisotropy, and selectivity, determine the reactor configuration, dimensions, and operating parameters to achieve the task. Collections of papers on plasma modeling and simulation can be found in special issues of IEEE Transactions on Plasma Science.[1]

5.1. Disparate length and time scales

One of the central issues in modeling the behavior of plasma processes is the disparity in length and time scales (Fig. 5; see also Fig. 1). Length scales range from atomistic, to microscopic (microfeature width), to mesoscopic (sheath, cluster of features) to macroscopic (reactor, wafer). Even if one focuses on reactor scale simulations, the presence of the extremely thin sheath in high-density plasmas introduces a wide range of length scales from hundreds of microns to tens of cm. The range of time scales is also extremely wide, from ps for the collision cascade, to the ns response time of electrons, to μs for positive ions, to tens to hundreds of ms for heavy species chemistry and gas residence times, to minutes for the duration of etching processes. One can extend the picture to include a process composed of several unit operations, or even the whole factory. When the whole range of scales is included, the problem becomes one of describing the behavior of an entire plant starting from molecular principles. This problem is unsolved at the present time, but given the rapid advancements in modeling and simulation at each individual scale, and the growth in computational power, one can envision that the overall coupled problem will be solvable within the next couple of decades.

A comprehensive plasma model should account for at least the following phenomena [29]:

1. Mass, momentum, and energy transport of charged and neutral species coupled with plasma chemistry.
2. The electric and magnetic field distribution in the reactor.
3. The variation of electron velocity distribution function with operating conditions.
4. Species transport in the sheath, and the resulting angular and energy distribution of ions, electrons, and any hot neutrals bombarding the surface.
5. Surface chemistry, especially ion-assisted reactions, recombination, or polymerization that might occur.

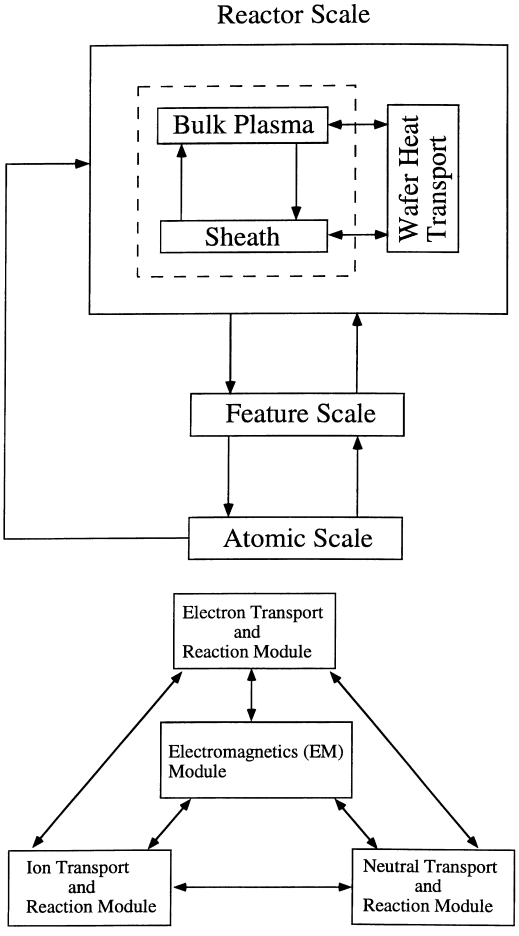

Fig. 6. A methodology for modeling plasma reactors by braking the problem into smaller parts. (Top) From the reactor, to the feature, to the atomic scale. (Bottom) Modules used for reactor scale model.

[1] See papers in special issues of IEEE Trans. Plasma Sci.: 19(2) (1991); 23(4) (1995); 14 (1986); 27(5) (1999).

6. Feature profile evolution.
7. Heat transport in the semiconductor wafer.

Because of the strong interaction and coupling of the phenomena enumerated above, performing a comprehensive multidimensional plasma simulation which couples all of these phenomena is an extremely challenging task, and is still an unsolved problem. One way to attack this problem is to break it down into smaller pieces, separating the length and time scales. An approach is shown in Fig. 6, top. The reactor scale simulation includes the bulk plasma and the sheath. Wafer heat transport should also be included here, although this item has not received attention in the literature, except for isolated cases [30]. Wafer (and/or reactor wall) heating is important as it can affect the rate of recombination, chemical etching and polymerization on the surface, as in the case of oxide etching. In many cases, bulk plasma and sheath are solved together, i.e. the same equation set is applied to the whole reactor. This approach is especially convenient for low plasma density systems in which the sheath thickness is an appreciable fraction of the reactor length scale [29], but has also been practiced, to a limited extend, in HDP reactors [31,32]. However, the most common approach for HDP systems (in which the sheath is extremely thin), is to solve the bulk plasma and the sheath separately [33–35], and then apply a 'splicing' procedure to connect the two [32,35]. The reactor scale model (or the sheath model if done separately from the bulk plasma) provides boundary conditions (species fluxes, energy and angular distributions) to the feature scale model. The surface chemistry model describes the reactions between neutral and charged particles with the surface, including ion-assisted chemistry, recombination, polymerization, or even secondary electron emission. This model can be phenomenological (Langmuir-Hinshelwood kinetics) or one based on molecular simulation approaches (Section 5.5). For example, molecular dynamics can be used to test the phenomenological Eq. (4) and to predict the value of the parameters in this equation. Of course experimental measurements (ion yields, reaction probabilities) should always be an integral part of surface chemistry modeling. The surface chemistry model is crucial for the feature evolution simulation.

The reactor scale model is further split into 'modules' (see Fig. 6, bottom) to separate the disparate time scales of electron, ion, and neutral transport. This is essentially an equation splitting approach. Calculation of the EVDF by solving the Boltzmann Eq. (3) is then part of the electron transport and reaction module. The EVDF determines the space- and time-dependent electron energy and transport properties (mobility, diffusivity), as well as the electron-particle reaction rate coefficients for given electric and magnetic fields and plasma gas composition profiles. The electromagnetics (EM) module solves for the electric and magnetic field distributions in the reactor using the Maxwell equations. The neutral and ionic species concentrations are obtained from the corresponding modules. Information is cycled among the modules until a converged solution has been obtained. There is no guarantee that the modular approach will converge, although it usually does so in practice.

Works done to connect the disparate length scales solve the problem in a sequential manner. For the plasma etching problem for example, Economou and Alkire solved for the macroscopic (reactor) scale [18] and used the results as a boundary condition for solving the sheath equation (mesoscopic scale) [36]. In turn they used the sheath simulation results as a boundary condition for the microscopic (feature) scale [37]. Feedback from the feature to the reactor was not considered. Lately, some progress has been made in self-consistent coupling (with feedback) of the disparate length scales of reactor (tens of cm) and microfeature (<1 μm) evolution in chemical vapor deposition CVD [38,39]. Gobbert et al. [38] developed a multiscale simulator that links the reactor and microfeature scales through a mesoscopic scale (~ few mm) model. The mesoscale corresponds to the size of a die on the wafer and contains clusters of microfeatures. Both reactor and mesoscale models were solved based on the continuum approximation (Knudsen number, $Kn = \lambda/L << 1$; here λ is the mean free path and L is a characteristic length scale of the system) using a finite element method, while the feature scale model was solved based on ballistic transport (no gas phase collisions). The calculation iterated among the different scale models until a converged solution was obtained. Thus, the effect of changing surface area, for example, due to microfeature shape evolution during CVD, could be accounted for in the simulation. Rodgers and Jensen also developed a multiscale simulator for CVD [39]. Feature scale Monte Carlo simulations were used to develop a 'surface reactivity' map as a function of location, $\varepsilon(r)$, which was used in the flux boundary condition for the reactor scale model. In this continuum finite element model the wafer surface was taken as planar. Information was exchanged back and forth between the models until convergence. Again, the effect of changing surface topography during CVD could be accounted for.

5.2. Reactor scale simulations

Plasma reactor simulations range from zero-dimensional (well-mixed) to three-dimensional. Well-mixed [40–42] and one-dimensional models (including plug flow models [43–45]) are best for sorting out the complicated gas and surface chemistry to arrive at a reduced reaction set for use in multidimensional simulations. Results of a 1D simulation of the species transport in a tube downstream of a plasma are shown in Fig. 7 [24]. This is part of a simulation of a downstream etching microwave plasma reactor at 525 mTorr pressure, 500 W power and 75 sccm flow of pure NF_3, used to etch silicon and its compounds (oxide, nitride). The species densities obtained by a well-mixed (0D)

model of the plasma zone were used as boundary condition at the inlet to the downstream section shown here. Due to its low dimensionality, the model can handle very complicated chemistry. Oxygen containing species originate from etching of the quartz walls. The F (etchant) density decreases downstream albeit slowly (Fig. 7, top) reflecting the low wall recombination efficiency of teflon coating the inner walls of the downstream tube. The charge densities decay much faster due to recombination at the tube walls (Fig. 7, bottom). The electron density is already very low compared to the negative ion density in the plasma (at $x = 0$) due to the strong electronegativity of the gas. Under these conditions, the ambipolar diffusion coefficient of charged species is much higher than what would be calculated for an electropositive plasma. The electron density plummets to very low values within a few mm of the source, and an ion-ion plasma is left to flow further downstream. The charged species diffusion in this plasma is essentially free diffusion. The calculations show that several cm of downstream section are enough to reduce the charged species density to very low values. In the actual reactor, wafers are tens of cm downstream, thus avoiding any charging damage of sensitive devices.

Two-dimensional simulations can address the important aspect of reaction uniformity across the wafer radius. Three-dimensional simulations are useful for studying azimuthal asymmetries in the reactor due to nonaxisymmetric power deposition, or nonaxisymmetric gas inlets and pumping ports [46,47].

Simulations of plasma reactors of the type used in the microelectronics industry started to appear only in the 1980s. A number of two-dimensional plasma reactor simulations were reported [18,48,49] focusing on the transport and reaction of neutrals only (neutral transport and reaction models). The electron density was assumed to have a uniform or Bessel function profile, and the electron energy was not calculated as a function of space and time in the reactor. The radical source terms (by electron-impact dissociation, for example) were estimated and the conservation equations for mass, momentum, and energy transport of neutrals were solved to obtain the fluid velocity profiles, gas temperature and the concentration distribution of radicals; this is a conventional computational fluid dynamics problem. Charged particle transport was not considered, and the effect of plasma gas composition (different than the feedstock gas composition) on the plasma properties was not accounted for. Aydil and Economou [50] improved on these works by using a well-mixed model for the discharge physics to obtain the electron density and electron impact reaction rate coefficients. These were used as input to a two-dimensional transport and reaction model to calculate etch uniformity. They also extended the model to include wafer heating effects [30].

Up until the early 1990s, simulations that solved for the radiofrequency (r.f.) plasma dynamics (so-called glow discharge models) were confined to one spatial dimension (1D) [51–59]. In addition, most of these simulations did not solve for the transport and reaction of neutrals, i.e. the effect of gas excitation and/or dissociation on the plasma characteristics was not accounted for. This can sometimes be a severe limitation since even minute quantities of excited species can alter the discharge properties [52]. Self-consistent r.f. plasma simulations which solve for the coupled effects of charged and neutral species transport and chemistry have only been reported within the past several years in 1D [52,53,57,58], 2D [29,31,60–64] and 3D [46,47]. Multidimensional simulations are particularly useful since they can address the important issue of plasma uniformity and the spatiotemporal plasma dynamics along both the radial and axial directions. However, most 2D simulations still do not include neutral transport and chemistry and consider noble gases (argon and helium) only [65–69], not reactive gas plasmas. Earlier simulations focused on capacitively coupled systems; recent studies focus on HDP systems. A review most relevant to ICPs is reported in [70].

There are three kinds of glow discharge simulations: fluid, kinetic and hybrid. Fluid simulations use moments of the Boltzmann Eq. (3) describing species density, momentum and energy conservation [27,71]. They require some assumptions regarding the species distribution func-

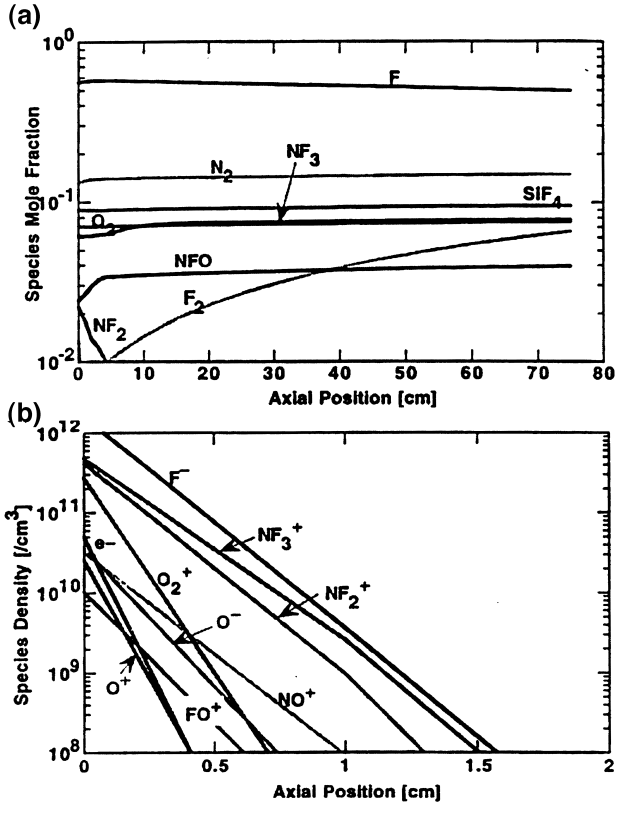

Fig. 7. Neutral (top) and charged (bottom) species mole fractions predicted by a 1D simulation as a function of distance downstream of a microwave plasma source. 525 mTorr pressure, 75 sccm of NF_3, 500 W power. Oxygen-containing species originate due to etching of the quartz tube containing the plasma. After Ref. [24].

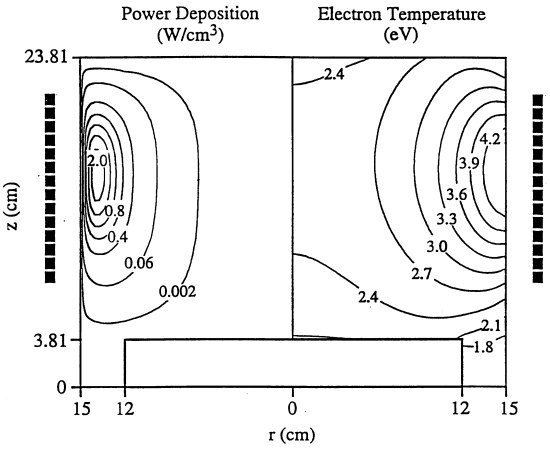

Fig. 8. Power density deposition profile (left) and electron temperature profile (right) for a total power of 3560 W, 10 mTorr, 200 sccm Cl_2 flow and 13.56 MHz coil excitation frequency. After Ref. [31].

tion to achieve closure of the equations. An electromagnetics module is also required to compute the power depositions profiles. The set of equations along with the corresponding boundary conditions describing this type of simulation has been given in numerous articles [61–64] and will not be repeated here. For most conditions of interest, the flow is laminar (Reynolds number <1) and diffusive (Peclet number <1) except for the gas inlet ports where convective velocities can be high. Judicious approximations can be made [70] to reduce the computational burden and arrive at TCAD (Technology Computer-Aided Design) simulation tools [33,70,72,73]. These references and others [61,63,64] also show comparisons of model predictions with experimental data.

Example results from a two-dimensional fluid simulation of polysilicon etching in an ICP with a solenoidal coil are shown in Fig. 8 [31]. Conditions were, 10 mTorr total pressure, 3560 W inductive power, 200 sccm of Cl_2 feed, and 13.46 MHz coil frequency with grounded substrate. The power deposition profiles are seen in Fig. 8, left. Most of the power is deposited near the coil, since the electromagnetic wave cannot penetrate the high-density plasma deeper than a few skin depths. The peak power deposition is greater than 2 W/cm^3; when averaged over the reactor volume the power deposition becomes 0.24 W/cm^3. The electron temperature distribution is shown in Fig. 8, right. Although the power is deposited only over a narrow toroidal zone, thermal conduction at the low operating pressure helps in heating up the whole plasma. However, the electron temperature distribution is quite nonuniform, because the electron energy relaxation length is shorter that the reactor dimensions [70]. The electron temperature is highest near the coil where the power deposited per electron is highest. The electrons cool down substantially in the narrow annular region between the substrate platen and the outer wall (lower right corner). Higher pressures tend to produce larger electron temperature variations. Lower pressures tend to increase the energy relaxation length and thermal conductivity thus making the electron temperature less nonuniform.

The majority positive ion (Cl^+) and electron density distributions are shown in Fig. 9. The peak ion density is nearly 4×10^{11}cm^{-3}. An off-axis maximum in the densities is observed which is further away from the coil compared to the ionization maximum (not shown). The charged species densities decay rapidly towards the walls. However, in contrast to low plasma density capacitively coupled reactors, the electron density is quite high even very near the wall. This is because the sheaths are thin due to the small (tens of microns) Debye length and the absence of high voltages across the sheath. The density gradients are steeper near the radial wall in the power deposition zone. Interestingly, the radial ion density profile changes from one with an off-axis peak near the axial midplane of the reactor to one with an on-axis peak near the wafer. In general, the positive ion spatial density profile depends on the values of power deposition, pressure, and reactor aspect ratio (radius/height). High values of these quantities favor off-axis maxima, low values favor maxima on-axis.

Next, an example from a reactor simulation of oxide etching in C_2F_6 plasma is given [74]. The chemistry of oxide etching is very complicated. Feedstock gases are dissociated in the plasma to produce fluorocarbon radicals (CF_x) and ions (CF_x^+). Radicals tend to deposit a fluorocarbon polymer layer on nonoxide surfaces (e.g. silicon), or on oxide surfaces not exposed to energetic ion bombardment (e.g. the sidewalls of a trench). The polymer does not form at the bottom of the trench on the oxide because ion bombardment induces reaction of the polymer-forming radicals volatilizing carbon as CO/CO_2 and also forming silicon fluoride product, thus etching oxide. In contrast, there is no efficient mechanism for carbon removal from silicon or nitride since they do not contain oxygen. Fig. 10 (top) shows the total ion flux impinging on an oxide covered, 200 mm- diameter wafer for three different pressures for an inductive (source)

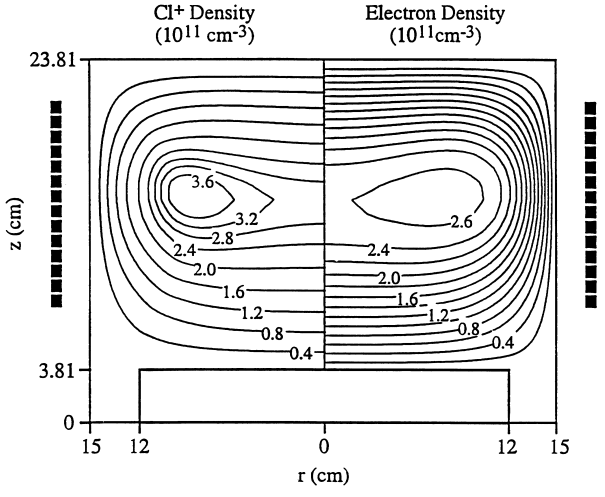

Fig. 9. Cl^+ ion (left) and electron (right) density profiles under the conditions of Fig. 7. After Ref. [31].

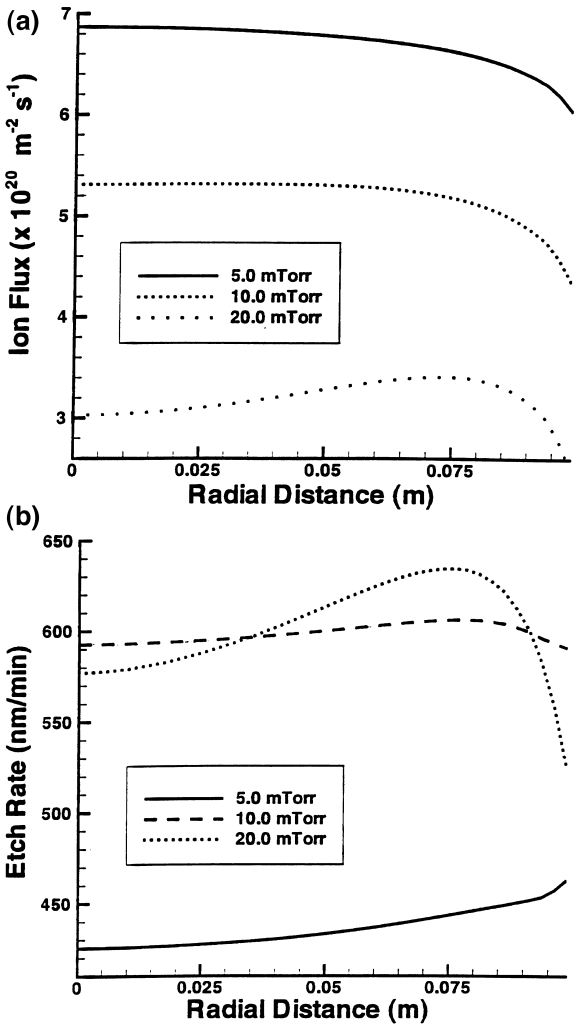

Fig. 10. (Top) Ion flux to an oxide-covered wafer etching in a C_2F_6 ICP with solenoidal coils, for three different pressures. Other conditions: coil power 2600 W, ion bombardment energy 370 eV, C_2F_6 gas flow rate 36 sccm. (Bottom) Oxide etch rate under the same conditions. After Ref. [74].

power of 2600 W. The ion flux is given by the product of the ion density at the sheath edge n_i, and the ion Bohm velocity, $J = n_i\sqrt{T_e/m_i}$. Here T_e is the electron temperature and m_i is the ion mass. The peak ion density actually increases with pressure (not shown) because of the higher concentration of neutral atoms available for ionization, and reduced diffusion losses of ions to the walls of the reactor. These two effects more than counterbalance the reduction in electron temperature (and ionization rate coefficient) with increased pressure. However, the ion flux at the wafer surface decreases with pressure because of stronger density gradients, and reduced T_e (thus reduced J_i) as pressure increases. The ion flux uniformity along the wafer surface also depends on pressure. The ion flux peaks on-axis for low pressures (5 mTorr) and off-axis for higher pressures (20 mTorr). Fig. 10 (bottom) shows the etch rate distribution along the surface of the oxide covered wafer for the same three pressures. The ion bombardment energy was 370 eV. Oxide etching is ion driven, yet the etch rates do not follow the ion flux trends; the etch rate is lowest at 5 mTorr at which the ion flux is largest. This is due to neutral chemistry. At 5 mTorr the surface is neutral starved. As pressure increases, the surface coverage of reactive radicals increases bringing about an increase in etch rate. This demonstrates that under conditions relevant to oxide etching in HDPs, oxide etching can be ion driven but neutral controlled.

Fig. 11 shows azimuthal asymmetries of etch rate of a polysilicon wafer in a 5 mTorr chlorine HDP predicted with a 3D fluid simulation [46]. The measured etch rate (a), should be compared to the predicted ion flux (c) profiles for a reactor with a one-turn planar coil (stove-top) antenna. Panels b and d correspond to a five-turn coil antenna. The close correspondence between measurements and predictions indicates that etching is ion controlled. The azimuthal asymmetries are due to azimuthal non-uniformities of power coupling to the plasma by the antenna. Non-uniform power deposition results in nonuniform plasma generation and azimuthal variations in plasma density profiles that carry over down to the wafer level. A five turn coil alleviates these azimuthal nonuniformities. The coil termination impedance also has a significant impact [46].

Kinetic simulations yield the particle distribution functions as an output of the simulation. They are considered more accurate than fluid simulations at low pressures when the species mean free path is comparable to or longer than a characteristic length scale ($Kn > 0.2$) or for highly nonequilibrium situations. However, there is evidence that fluid simulations can perform well even at low pressures for which their assumptions must be scrutinized [75]. Kinetic simulations are computationally intensive as compared to fluid simulations. They include Particle-In-Cell with Monte Carlo Collisions (PIC-MCC) [76,77], Direct Simulation Monte Carlo (DSMC) [78–80], and Dynamic Monte Carlo [81] approaches.[2]

DSMC was first developed for the direct simulation of rarefied gas flows. The flow domain is divided in a number of cells. The cell size is determined by the local mean free path λ; a size $\sim\lambda/3$ is typically recommended. The actual flow field is simulated using a number of particles (simulated molecules); some 10^7 particles are not atypical for runs on massively parallel supercomputers. The type, spatial coordinates, velocity components, internal energy, and weight factor of each simulated molecule are stored in the computer. The weight factor is the number of real molecules represented by each simulated molecule. As the molecules move through the reactor, molecules collide with one another and with the walls of the container. Feed molecules may be introduced at specified inlet port locations, and

[2] Note that the PIC-MC simulation in Ref. [81] is not self-consistent. The electric field profiles were obtained by the fluid simulation and then used to move particles. For that reason, the species densities and energies predicted by the PIC simulation are modulated excessively in the bulk; for example, compare Fig. 7a,b of Ref. [81].

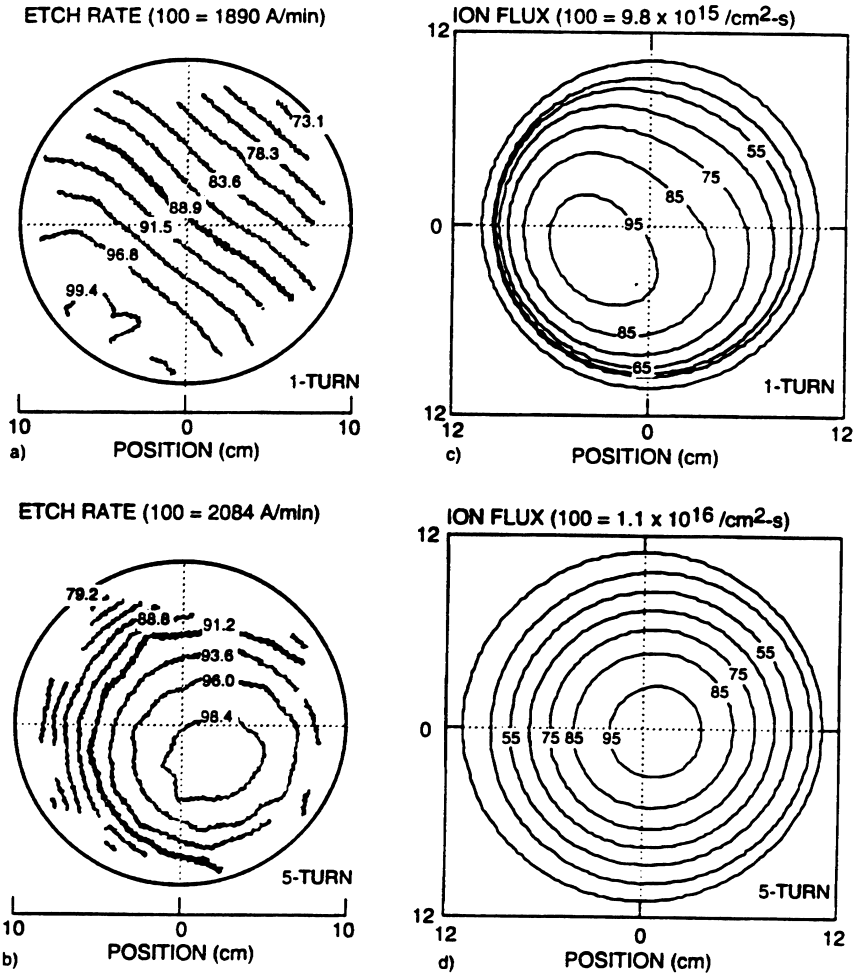

Fig. 11. Measured etch rate distribution on a polysilicon-covered 200 mm diameter wafer etched in an ICP reactor with a one-turn (a) and a five-turn (b) stove-top coil. Calculated ion flux profiles on the wafer for the one-turn (c) and the five-turn (d) coil configurations, respectively. Conditions: 200 W and 5 mTorr.

molecules may be removed from the simulation because of chemical reactions (in which case their identity changes) or through the pumping ports. The basic premise of DSMC is that the motion of simulated molecules can be decoupled from their collisions over a time step. The size of the time step is selected to be a small fraction of the mean collision time, or a fraction of the transit time of a molecule through a cell. During the motion phase, molecules move in free flight according to their starting velocity and the forces acting on the molecules (e.g. electric field force on ionized species). During this phase, molecules may cross cell boundaries, collide with walls, or exit the flow field. During the collision phase, collision pairs are selected from within each cell regardless of the position of the molecules within the cell. It is imperative that the collision frequency occurring in the actual flow field is simulated correctly. One should note that DSMC is limited to binary collisions. This does not pose a problem for the low pressure simulations of interest. DSMC should be distinguished from the 'test particle' Monte Carlo method. The latter is used to track the motion of a test molecule through a flow field established by some other means (e.g. a fluid simulation). The test molecule does not influence that flow field. Statistics are collected by following the trajectories of many test molecules. In DSMC, each and every molecule can influence the flow of the other molecules; i.e. the flow field is the result of the collective behavior of all molecules.

In PIC-MCC [76] a mesh (grid) is overlaying all the particles (the computational domain). Based on the particle positions, charges are assigned to each mesh point and current densities are assigned to the faces between the mesh points (weighting). Maxwell's equations are then solved to compute the electric and magnetic fields on the grid. The force on the particles is obtained from the fields at these gird points by interpolation based on the particle position (another weighting). Particles are then moved according to Newton's law (deterministically). Particle collisions are handled stochastically in a Monte Carlo module in-between field adjusting time steps. Typically, the null-collision method [82] is used for computational efficiency. A more efficient and less restrictive method to handle collisions is the Dynamic Monte Carlo DMC simulation method

[81]. In contrast to the null collision technique, DMC does not require the free flight distribution as input to the simulation and requires fewer random numbers. In fact, the free flight distribution is an output of DMC.

Hybrid simulations have been developed [61,64,83] in an attempt to preserve the accuracy of kinetic simulations and at the same time reduce the computational burden. A common hybrid procedure is to obtain the electron transport (mobility, diffusivity) and reaction rate coefficients (e.g. ionization rate) by solving the Boltzmann Eq. (3) via a Monte Carlo method [61,64]. These are then used in the species mass and momentum continuity equations to obtain species densities and fluxes. Monte Carlo simulations of multidimensional EVDFs (or the respective electron reaction rate coefficients) can be time-consuming. Spatial averaging of the distribution function under the so called nonlocal condition [84] can offer great simplifications. The nonlocal approach for electrons was combined with a fluid approach for ions (a hybrid) to yield a rapid 2-D argon discharge simulation [83].

Recently, it has been recognized that pulsed plasma operation (in which the plasma power is modulated with a given period and duty cycle) can ameliorate anomalous etch profiles (e.g. notching) and other undesirable effects that occur in conventional continuous wave (cw) discharges. Due to the large difference in electron and ion temperatures in a cw discharge, positive ions bombarding the wafer have a strongly anisotropic velocity distribution, while that of electrons is almost isotropic. As a result, positive ions can penetrate deeply into a trench charging the trench bottom positively, while electrons deposit their charge on the sidewalls of the trench. Such charging, and the associated etch profile distortion, have become a major problem for the fabrication of the next generation of microdevices.

The situation becomes more favorable in pulsed-power discharges [85,86]. Recent studies indicate that extraction of charged species from the afterglow plasma and their acceleration towards a r.f.-biased electrode could dramatically reduce charging damage and improve etching characteristics. For instance, greatly improved etch performance has been reported in pulsed-power chlorine discharges by applying a low frequency bias to the substrate in the afterglow of an inductively coupled plasma source. It was suggested that low frequency bias results in alternate acceleration of positive and negative ions extracted out of the plasma. Since positive and negative ions have almost equal masses and similar velocity anisotropy under the influence of r.f. bias, the net charge deposited on the wafer surface is almost zero, minimizing charge-induced damage. However, there has been no direct proof that negative ions are involved in etching.

Fig. 12 shows the results of a 1D simulation of a high-density pulsed plasma in chlorine [43]. The pulse period was 100 μs and the duty cycle was 50%. The power density was 1.0 W/cm^3 and the pressure was 20 mTorr. The negative ion Cl^- (chlorine negative ion) density is comparable to the

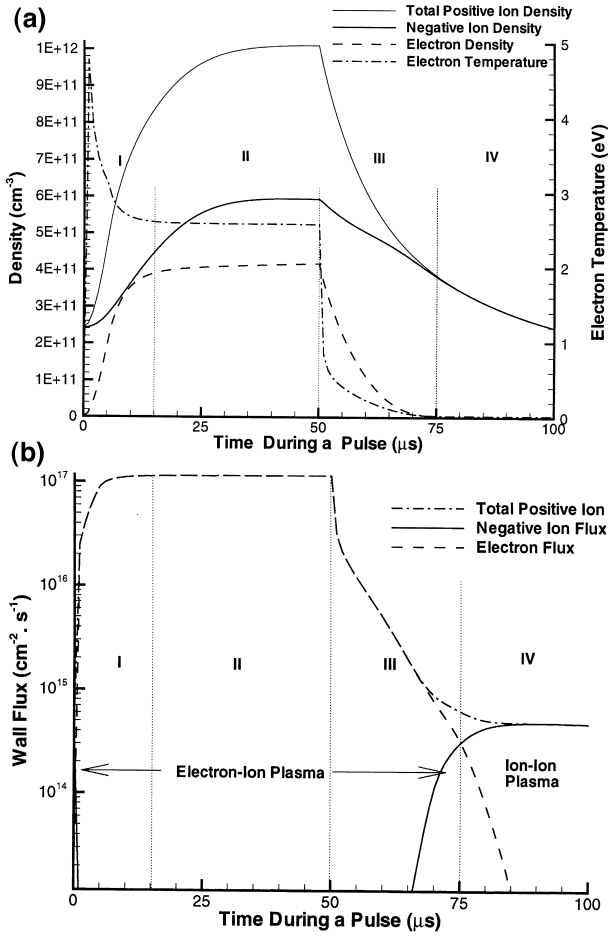

Fig. 12. Time variation of species densities (top) and fluxes (bottom) predicted by a 1D model of a high-density pulsed plasma through chlorine. Power 1.0 W/cm^3, pressure 20 mTorr, pulse period 100 μs, duty cycle 50%, wall recombination probability of Cl atoms 0.1. After Ref. [43].

electron density during the plasma-on phase, and exceeds greatly the electron density during plasma-off. When power to the plasma is turned off (at 50 μs), electrons cool down (T_e decreases) and are lost by dissociative attachment to molecular chlorine to form Cl^-, and by diffusion to the walls. At the same time the sheath potential collapses, and late enough in the afterglow the electron density has decreased to very low values, leaving behind what is essentially a positive ion–negative ion (ion–ion) plasma (phase IV shown in Fig. 12). When the sheath potential becomes comparable to the negative ion thermal energy, negative ions can leave the plasma. This is reflected in the time evolution of the particle fluxes (Fig. 12, bottom). When the plasma is on the sheath potential is large enough (several kT_e) to be able to contain all negative ions in the plasma.

5.3. Sheath simulations

Typical events that can occur in the sheath are as follows. (a) Fast electrons from the plasma can overcome the (decelerating) sheath potential and reach the wall. In fact, such

electron current is necessary to neutralize the positive ion current to the wall. (b) Slow electrons are reflected back into the plasma. (c) Negative ions cannot penetrate as far as electrons (because of the much lower energy of the negative ions) and are also reflected. (d) Positive ions are accelerated by the sheath field. In their transit through the sheath, positive ions can suffer elastic scattering or charge exchange collisions, or engage in chemical reactions with neutrals. (e) Collisions lower the energy of ions bombarding the electrode to below the sheath potential. (f) Secondary electrons can be emitted as a result of ion bombardment, which are then accelerated back into the plasma, performing ionization of neutrals on the way.

A variety of models of the DC sheath have been published that make different assumptions regarding ion flow (collisional vs. collisionless), presence or absence of electrons (including secondary electrons), and the form of the boundary conditions. Both fluid [36,87,88] and kinetic models [89,90] have been developed. Some of these are used to describe the high-frequency r.f. sheath, when ions respond to the time-average (a DC) voltage [36]. The ion energy distribution at the wafer is an important factor in determining the rate of surface reactions in plasma processing (Eq. (4)). Ions falling through a DC sheath without collisions will acquire the full sheath potential. For a sheath potential much larger than the electron temperature (the latter expressed in volts), the ions bombarding the wall will be almost monoenergetic. Ion-neutral collisions will lower the ion impact energy and result in an ion energy distribution (IED) function.

Plasma processing reactors normally operate with the wafer biased at radio frequencies, typically in the range 0.1 to 13.56 MHz. The literature on r.f. sheaths is voluminous. Both fluid [91–93] and kinetic (e.g. solution of the Boltzmann equation or Monte Carlo) [94–97] simulations have been reported. One of the most important results of such simulations is the IED [98]. The ion angular distribution (IAD) and sheath impedance (for use in equivalent circuit models) are also of importance.

Even if the ions injected at the sheath edge were monoenergetic, an IED would result from an r.f. (time-dependent) sheath, even in the absence of collisions. The critical parameter that controls ion modulation in r.f. sheaths is $\omega\tau_i$, where ω is the frequency of the applied field, and τ_i is the ion transit time through the sheath [96,97], $\tau_i = 3s\sqrt{m_i/(2eV_{sh})}$, where s is the sheath thickness, m_i is the ion mass, V_{sh} is the sheath voltage. When $\omega\tau_i << 1$ ions traverse the sheath in a short time compared to the field oscillations. Under this condition, an ion traversing the sheath experiences the sheath voltage prevailing at the time the ion entered the sheath. The IED function will reflect precisely the variation of the sheath voltage with time. This quasi steady-state condition of $\omega\tau_i << 1$ is satisfied for low r.f. frequencies or short ion transit times, i.e. thin sheaths (low sheath voltage or small Debye length), or ions of small mass. At the other extreme of $\omega\tau_i >> 1$, ions experience many field oscillations while in transit through the sheath. Ions will then respond to the time-average sheath potential, and the IED function will have a smaller spread over energy. The two extreme conditions are more amenable to analysis since, in both cases, the sheath can be described as a DC sheath; actually a series of DC sheaths at the different moments in time during the r.f. cycle when $\omega\tau_i << 1$, and a DC sheath at the time-average voltage when $\omega\tau_i >> 1$. The most difficult situation to analyze is when $\omega\tau_i \approx 1$. Monte Carlo simulations [96,97] as well as fluid simulations [99,100] have been performed in this intermediate regime.

Fig. 13 (top) shows the energy distribution of several ions impinging on the grounded electrode of a 13.56 MHz r.f. discharge [7]. In this case the sheath potential is identical to the plasma potential. Heavy ions (Eu^+) have a long transit time corresponding to $\omega\tau_i > 1$. Their IED is narrow and corresponds to the time-average plasma potential (about 100 V in this case). As the ion mass and transit time decrease ($\omega\tau_i < 1$), the IED becomes wider and reflects more and more the time-dependence of the plasma potential. Theory predicts that the energy spread ΔE should scale as $m_i^{-0.5}$ [98,100]. The measurements are in reasonable agreement with this expectation. The calculated IED on a biased electrode immersed in a high-density argon discharge for different applied frequencies is shown in Fig. 13 (bottom) [100]. The electron temperature was 3 eV, and the plasma

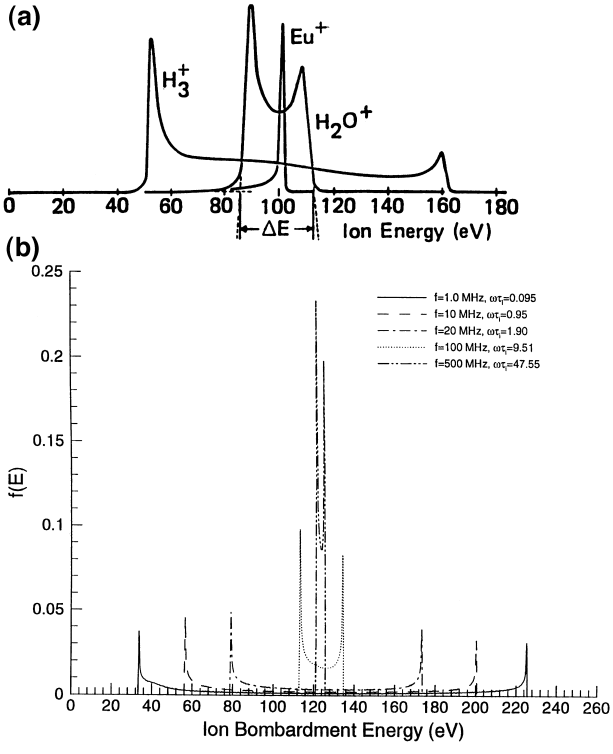

Fig. 13. (Top) Measured ion energy distributions (IED) at a grounded wall for ions of different masses crossing a r.f. sheath over that wall. The energy spread is reduced as the ion mass increases. After Ref. [7]. (Bottom) Calculated IED for Ar^+ ions bombarding an electrode immersed in a high-density argon plasma for different excitation frequencies. After Ref. [100].

density at the sheath edge was 6×10^{10} cm^3. As the applied frequency is increased the energy dispersion decreases. The low energy peak of the IED is higher than the high-energy peak. At low frequencies, the IED corresponds directly to the time variation of the sheath potential. At very high frequencies, ions tend to follow the average sheath potential and the two peaks of the IED tend to merge.

5.4. Microfeature simulations

The ultimate goal of plasma etching is to obtain controlled wall profiles of microscopic features etched into a film. Anisotropic etching refers to the situation where reaction proceeds only along the bottom surface of a microscopic feature, or more precisely, only along surfaces that are not perpendicular to the macroscopic wafer surface. Anisotropic etching is based on the premise that energetic ion bombardment is directed along the normal to the wafer surface. Of course, the finite ion temperature can result in a spread of ion velocities around the surface normal. Plasma etching processes are designed to minimize this angular distribution of ion flux. Also, the ion energy must be optimized in the sense that it should be enough to cause the desired surface reaction but not too high to cause undesired sputtering or radiation damage. In many cases that optimum lies in the range of 50–300 eV, depending on the system. There are basically two mechanisms to achieve anisotropy. When gasification of the solid by neutral species is not spontaneous, etching can occur only on surfaces exposed to ion bombardment (ion-induced etching). Thus, anisotropy can be readily achieved. However, when the chemical reaction between neutrals and the surface is spontaneous, a 'wall passivation' mechanism is necessary to achieve anisotropy. Wall passivation means deposition of thin polymeric films or 'inhibitors' that block etching of the surface by the neutrals. The passivation film does not form on surfaces exposed to ion bombardment, allowing etching to proceed unimpeded on these surfaces. The deposition of passivation films is controlled by judicious selection of the plasma chemistry and wafer temperature. Oftentimes, the photoresist (polymer) used as mask contributes to the formation of passivation films. Spontaneous chemical etching can be stopped, even without a passivation layer, if the wafer is chilled to low enough temperatures to quench the reaction.

The minimum feature width is rapidly falling below 0.25 μm in modern microelectronic devices, and the typical aspect ratio of features will soon become greater than 10:1 (see for example *The National Technology Roadmap for Semiconductors* published by the Semiconductor Industry Association in San Jose, CA). Etching narrow, high aspect ratio features in a reproducible manner in a manufacturing environment is a very challenging task. The problem is complicated by the fact that, frequently, features of different aspect ratios have to be etched on the same wafer in the same plasma. If the etch rate depends on aspect ratio (aspect ratio depended etching, ARDE), overetching of some regions of the wafer will be required which can lead to profile distortion and device damage. In ARDE [101,102] the etch rate decreases as the trench aspect ratio increases (also known as RIE lag). ARDE can occur due to a combination of effects. As the trench becomes deeper, for example, ions may impact the sidewall instead of the trench bottom. This can be due to the angular distribution of the incoming ion flux, or the decollimation of ions due to local electric fields developed by nonuniform charging of the mask or the trench sidewalls. As the flux of ions impinging on the trench bottom decreases, the etch rate follows suit. Also, transport limitations may reduce the flux of neutrals reaching the bottom of the trench for high aspect ratio trenches. Finally, in a less common situation, the etch rate increases as the trench deepens (inverse RIE lag).

In another situation encountered in oxide etch, etching of high aspect ratio trenches stops altogether due to accumulation of polymer at the bottom of the trench (etch stop). Oxide etching is ion driven. The etch rate of a flat (no features) bare oxide surface as a function of ion energy in a CHF_3 inductively coupled plasma is shown in Fig. 14 [103]. The ion energy was varied independently by applying a bias to the substrate electrode. All other conditions (including coil power generating the plasma) were kept fixed. At low ion bombardment energies (polymer deposition regime) there is actually polymer depositing on the oxide. Interestingly, initially there is an increase in the polymer deposition rate as the ion energy is increased. This corresponds to ion-enhanced deposition. Apparently, low energy ions create more dangling bonds (surface sites) on the polymer surface that enhance the deposition rate. As the ion energy is increased further (polymer suppression regime), polymer deposition competes with polymer (chemically-enhanced) sputtering; eventually sputtering wins and beyond an ion energy of ~60 eV there is net oxide etching. In the etching regime, the oxide etch rate increases with ion energy following approximately the square root law (Eq. (4)). In more polymerizing chemistries (lower F/C ratio [104]), more energetic ions would be needed to suppress polymer formation and sustain etching. Now, ions moving down the trench can be decelerated because of positive charging of the walls deeper inside the trench (see below); the ion energy may then fall below the value needed to sustain etching. Also, wall reactions may change the radical mix to a more polymerizing system as radicals diffuse (Knudsen diffusion) down the trench. Finally, 'seasoning' of the reactor walls can alter the wall recombination probability of radicals, again affecting the radical mix. These factors are important in explaining oxide etch stop in high aspect ratio features.

The shape of an etched feature depends on a plethora of geometric, material, and plasma parameters. The shape evolution problem is coupled to the plasma reactor through the sheath (Fig. 6, top). Feedback from the feature to the reactor occurs through the flux of product species coming

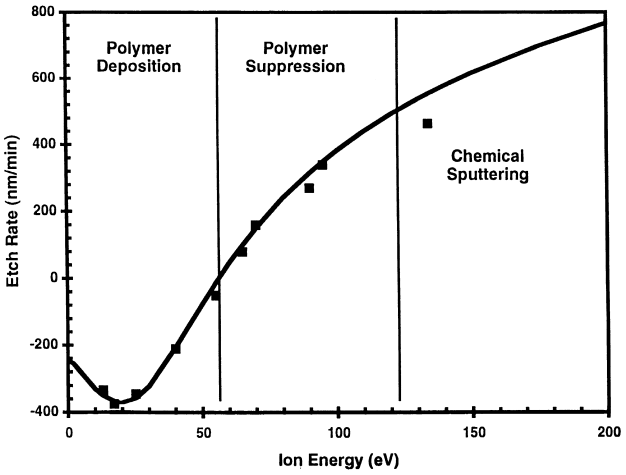

Fig. 14. Oxide etch rate as a function of ion bombardment energy After Ref. [103]. Three regimes are shown: (points) polymer deposition, polymer suppression, and chemical sputtering. Solid line is model prediction [74].

out of the feature and the varying surface area available for reaction as the feature shape evolves. The former affects the plasma gas composition and in turn the flux and energy distribution of species incident on the feature. The latter can be important, for example, when loading is present. Also, the reaction products can affect selectivity, as in the case of silicon etching in bromine and chlorine containing plasmas [105]. Apparently, silicon chlorides can be fast oxide etchants under certain conditions degrading the silicon to oxide selectivity.

Another issue which is becoming more important as the feature aspect ratio increases is that of charging damage resulting from ion and electron bombardment of the wafer. One form of damage is the so-called notching [106–108] observed in etching of polysilicon lines over oxide. Because ions coming out of a plasma are much more directional than electrons, the sidewalls of a microfeature charge negatively while its bottom charges positively. Further ions coming into the feature are deflected by the charge deposited on the surface, and their trajectories are bent to the point that these ions induce etching of the polysilicon sidewall. This distortion of the sidewall profile (notching) is highly undesirable. Charging and ion deflection are also suspected to be responsible for ARDE. Another form of charging damage is gate oxide breakdown because of large currents flowing through the oxide in a nonuniform plasma. In order to simulate charging damage and profile evolution of microfeatures, the multidimensional electric field profiles near the trench must be calculated.

The forward problem from the reactor to the feature, ignoring the coupling back into the reactor, was considered by Economou and Alkire [37], and later by Kinoshita et al. [107], and Hwang and Giapis [108]. Because of the disparity of the length scales involved, it helps to break down the problem into smaller pieces. The near wafer space is separated into two regions, Region I and Region II. Region I contains the sheath except for the immediate vicinity to the features which is designated as Region II. Since the sheath is much thicker than the feature size and, at the same time, much thinner than the wafer size, a one-dimensional sheath model suffices for Region I. Region I (sheath) contains a net space charge, hence the Poisson equation has to be solved for that Region. The boundary conditions at the sheath/plasma interface are the electron and ion densities, and the electron temperature (or the velocity distribution functions) of these species. A one-dimensional sheath simulation yields the density, energy, and angular distribution of the charged species leaving Region I and entering Region II. Region II, in the immediate vicinity of the feature, has to be described by at least a two-dimensional electric field model. The species trajectories, as influenced by this field, are followed in Region II until species strike the wall and deposit their charge. Owing to the very low charge density near the feature, the Poisson equation can be replaced by Laplace's equation in that region. As charges accumulate on the wall, the wall potential is modified and Laplace's equation has to be solved iteratively in Region II until a steady state is reached. The time constant to approach the steady state is a few ms, much faster that the time scale of shape evolution [108]. Knowing the flux and energy of ions striking the walls, the local etch rate can be calculated (assuming a reaction yield), the wall profile advanced, and the charging calculation repeated until the feature is etched to the desired depth [107–109].

In general, in order to perform a shape evolution calculation one needs to have information on the following.

(a) The flux, energy distribution, and angular distribution of ions and neutrals along the wall as a function of the instantaneous shape of the feature. As explained above, charged species trajectories can be deflected by local charging of the walls. Neutral species flux variations can also exist along the walls. For example, if the neutrals react with high probability, the neutral flux will be determined by the line of sight flux reaching the surface (neutral shadowing); or Knudsen diffusion will lower the concentration of neutrals deep inside high aspect ratio trenches.
(b) Etch rate of the materials involved (film to be etched, mask) for given neutral-to-ion flux ratio and angle of incidence of the ions.
(c) The energy and angular distribution of energetic ions (and possibly energetic neutrals) reflected off of the walls. These species may have substantial energy (especially when they strike the wall at glancing angles) and they can do further chemistry when striking the wall again.
(d) The reaction or sticking probability of products evolving from the feature walls.
(e) The surface diffusivity of adsorbed species and surface conduction of charge.

Data needed to perform profile evolution simulations may be obtained by well-defined experiments. A set of such experimental data designed to measure the etch yield of

polysilicon is shown in Fig. 15 [19]. An undoped polysilicon sample was bombarded simultaneously by separate beams of Cl radicals and Cl^+ ions of controlled flux and energy. The silicon etching yield (silicon atoms removed per incident ion) was found to depend on the ratio of neutral to ion fluxes. Exposure of the sample to the radical beam alone did not produce any appreciable etching under these low temperature conditions. The etching yield increases with ion energy; it turns out that the ion energy dependence is given by Eq. (4). For a given ion energy the yield is linear with flux ratio (FR) for low values of FR, and saturates for high FR. For low FR, etching is limited by the neutral flux; there is simply not enough reactant (chlorine) to form product, and the Cl surface coverage is expected to be low. At high FR, the surface is expected to be fully covered with chlorine, and etching is limited by the ion flux. Actually, since ion bombardment forms a damaged layer on top of silicon, the chlorine coverage is more than a monolayer. The beam experiment shown in Fig. 15 is most relevant to polysilicon etching in high-density plasma sources where the molecular chlorine dissociation is high. Hence, most of the reactant is Cl and the corresponding ion in the plasma is Cl^+. However, similar effects are observed when silicon is bombarded by a molecular chlorine beam (instead of Cl) and an argon or Cl_2^+ beam (instead of Cl^+), except that in these cases the etch yield is lower. For given ion energy and neutral to ion flux ratio, the polysilicon etching yield decreases monotonically with angle of incidence of the Cl^+ ion beam measured from the surface normal [19]. The angular dependence of the yield is needed to calculate the evolution of the profile of microfeatures during etching.

The shape evolution of microfeatures is followed using a

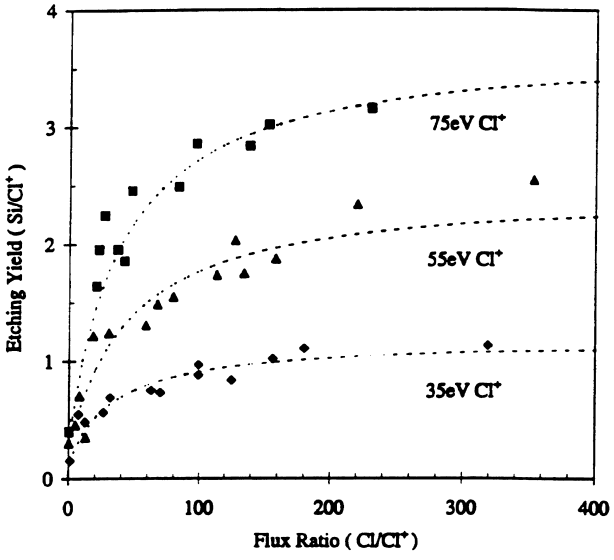

Fig. 15. Etching yield of silicon bombarded by a Cl atom beam simultaneously with a Cl^+ ion beam of controlled energy. At low values of the flux ratio, etching is limited by Cl atom supply. At the other extreme, etching is limited by the ion flux. Dashed lines are the result of a Langmuir–Hinshelwood model of the surface reaction. After Ref. [19].

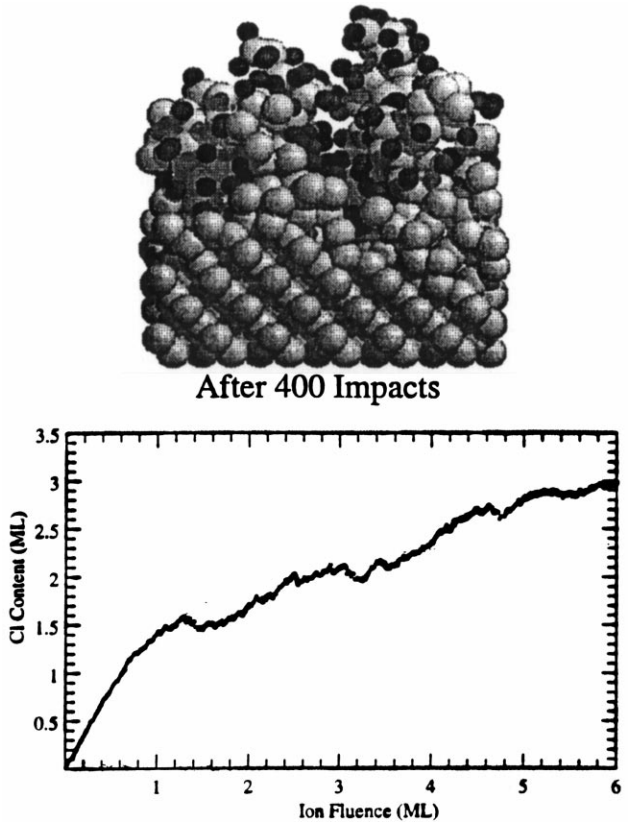

Fig. 16. (Top) Side view of an initially perfect (100) silicon lattice bombarded consecutively by a dose of 5.5 monolayers of 50-eV Cl_2^+ ions impinging perpendicular to the surface and starting from random locations above the lattice. (right) chlorine uptake as a function of dose of an initially perfect (100) silicon lattice. After Ref. [132].

number of techniques. The string model was popular at first [110], but profile advancement based on the method of characteristics [111] is more robust. In another method [112] the solid is divided into a large number of elements (digitized). The volume 'digits' are removed (etching) based on the local etch rate and a local mass balance. If deposition takes place a volume element is added locally. Unfortunately, items (b)–(e) above are largely unknown for almost all material systems. Surface chemistry in particular is one of the major limitations of current models of profile evolution. One is then forced to use a number of adjustable parameters that limit the predictive value of the model. A plethora of profile evolution simulation results have been published in the literature [113–119].

5.5. Atomistic simulations

Atomistic simulations provide information at the molecular level. Such information is useful for understanding the progress of an event occurring in the gas phase or on the surface, for delineating reaction mechanisms and pathways, for calculating rate coefficients of difficult to measure reactions, and for enhancing one's understanding of the process by visualizing the atomic scale events. Molecular modeling

techniques include ab initio methods (e.g. density functional theory, DFT) of electronic structure and total-energy calculations [120,121], and semi-empirical and empirical atomic-scale simulations (e.g. Molecular Dynamics, MD, and Monte Carlo, MC [122–124]).

MD simulations are suitable for studying the interaction of energetic ions with solids. MD follows the trajectory of each atom in the simulation cell as a function of time for several ps of the ion–solid interaction by solving Newton's equation of motion for each atom. Physical quantities of interest may be calculated by time or ensemble averaging. The most critical input is the interatomic potential that is used to calculate the force on each atom. Reliable empirical potentials exist for common systems (e.g. silicon), but such potentials are, in general, not readily available. The MD simulation cell can contain millions of atoms, i.e. length scales >100 Å can be addressed. The current practical limit of time scales is ~100 ps. MD simulations have been used to study physical sputtering [125], physical vapor deposition [126], and the reaction of energetic neutrals with a surface in the absence of ion bombardment [127]. MD simulations have also been used to study the interaction of ions with Si under simultaneous exposure to chlorine [128], and fluorine [129], as would be the case in RIE. Finally, MD was employed to understand atomic scale events and surface reaction mechanisms during atomic layer etching of silicon [130,131].

Fig. 16 (top) shows a side-view image of a silicon surface bombarded with approximately 5.5 monolayer equivalents of 50 eV Cl_2^+ ions [132]. Significant roughness of the otherwise crystalline solid has been introduced by ion bombardment and chlorine has been incorporated to a depth of approximately 10 Å. The chlorine taken up by the surface as a function of ion fluence is shown at the bottom of the figure. The surface shows signs of saturation with about three monolayers of coverage. The thickness of the modified layer and the Cl saturation concentration are similar to the values measured by Layadi et al. [133]. The Cl-modified layer is important for reactive ion etching since the collision cascade due to ion bombardment can promote the formation of higher chlorides in this layer which eventually leave the surface as products. The near-surface (damaged) layer can be detected by spectroscopic ellipsometry, XPS, or laser-desorption/laser-induced-fluorescence (LD-LIF) measurements [133]. Under a set of typical operating conditions (100 sccm chlorine gas flow, 2 mTorr pressure, 200 eV ion bombardment energy) a steady-state surface layer forms within a few seconds after plasma exposure. The thickness of the surface layer, as determined by spectroscopic ellipsometry, is a linearly increasing function of ion (Cl^+ and Cl_2^+) bombardment energy [133]. As ion energy increases, ions are able to penetrate deeper inside the silicon lattice, thereby creating a thicker near surface (damaged) layer. The surface layer is in the range of 10–35 Å for ion energies ranging from 20 to 370 eV.

Kinetic Monte Carlo (MC) methods are also useful [134,135], but one needs to have a fairly complete idea of the physics and chemistry of the problem to apply them. For example, the types of possible events and the probability of occurrence of each event must be known, before the time evolution of the process can be simulated. MC can address much longer time scales compared to MD (e.g. diffusional or adsorption time scales). Combinations of MD and MC may be useful in simulating the range of time scales from atomic vibrations to surface chemical reactions.

6. Concluding remarks

Plasma processing will continue to be of critical importance for fabricating ULSI devices [136]. More complex patterns with finer dimensions down to a few hundred angstroms, as well as films with properties tailored to more specific applications, are expected in the future. These stringent requirements will necessitate integrated processing and process automation with sophisticated smart sensors for real-time process control. In particular, real-time surface sensors will be indispensable.

Multidimensional simulations of plasma reactors can serve as powerful tools for improving our understanding of reactive plasmas, and for helping in the design of new and improved plasma processes. Despite their young age, such simulations are already quite advanced. Further understanding of plasma physics and chemistry as well as developments in numerical methods and in parallel computing will have a profound impact on multidimensional simulations of glow discharges coupled with neutral transport and reaction, culminating in a virtual plasma reactor. This virtual reactor will be based on an integrated system approach in which the reactor design, control, and optimization problems are not solved separately but simultaneously. In general, a combination of well-defined experiments, plasma diagnostics [137–140] and mathematical modeling/simulation will continue to be the best approach in unraveling the intricacies of plasmas and the plasma–surface interactions.

Understanding at the molecular level will become increasingly important. The push for lower pressure to improve uniformity and ion directionality will necessitate the further use of 'particle' (DSMC or PIC-MCC) simulations. Surface processes including ion-assisted (or beam assisted in general) reaction kinetics, deposit nucleation and growth, and adhesion must be better understood to engineer materials and microstructures with tailored properties (e.g. superlattices). Hybrid Molecular Dynamics–Monte Carlo simulations (to cover both the ps time scale of events upon ion impact and the relaxation of the lattice after impact) coupled with well-defined beam experiments will provide much insight into the ion-assisted chemistry happening on surfaces exposed to plasmas. Atomic resolution techniques with capability of real time, in-situ monitoring such as scanning tunneling microscopy (STM) and

atomic force microscopy (AFM) will find increasingly more applications. Atomic layer processing [141], with the capability to control film deposition and etching with monolayer accuracy, will be further developed. Understanding the relation between processing–microstructure–properties of deposited films will result in much improved tailored materials.

Efficient treatment of the disparate length and time scales will be the key to the further development of predictive computational models for plasma engineering. This is not limited to the plasma process, however. It includes the solid materials produced or modified by these technologies; from the atomic level, to the microstructure to the bulk material properties. Finally, integration of modeling/simulation with design, sensors, control, optimization, safety and reliability will result in an ultimate integrated system which is based on molecular principles and which extends all the way to the factory scale!

Acknowledgements

The author would like to thank the National Science Foundation (CTS 9216023 and CTS 9713262), Sandia/SEMATECH, The Welch Foundation and the State of Texas (Texas Advanced Technology Program) for financial support of this work.

References

[1] S.M. Rossnagel, J.J. Cuomo, W.D. Westwood (Eds.), Handbook of Plasma Processing Technology Noyes, Park Ridge, NJ, 1990.
[2] M.A. Leiberman, A.J. Lichtenberg, Principles of Plasma Discharges and Materials Processing, Wiley, New York, 1994.
[3] B.M. Penetrante, S.E. Schultheis (Eds.), Nonthermal Plasma Techniques for Pollution Control, Parts A and B, Springer, New York, 1992.
[4] M. Konuma, Film Deposition by Plasma Techniques, Springer, New York, 1992.
[5] H. Yasuda, Plasma Polymerization, Academic Press, San Diego, CA, 1985.
[6] S.J. Fonash, J. Electrochem. Soc. 137 (1990) 3885.
[7] J.W. Coburn, E. Kay, J. Appl. Phys. 43 (1972) 4965.
[8] S.A. Cohen, in: D.M. Manos, D.L. Flamm (Eds.), Plasma Etching: An Introduction, Academic Press, San Diego, CA, 1989.
[9] T.J. Sommerer, M.J. Kushner, J. Appl. Phys. 70 (1991) 1240.
[10] L.G. Christophorou (Ed.), Electron–Molecule Interactions and their Applications, Vols. 1 and 2, Academic Press, New York, NY, 1984.
[11] V.E. Golant, A.P. Zhilinsky, I.E. Sakliarov, Fundamentals of Plasma Physics, Wiley, New York, 1980.
[12] I.P. Shkarofsky, T.W. Johnston, M.P. Bachynski, The Particle Kinetics of Plasmas, Addison-Wesley, Reading, MA, 1966.
[13] E. Meeks, P. Ho, Thin Solid Films (This issue) 334.
[14] D.L. Flamm, in: D.M. Manos, D.L. Flamm (Eds.), Plasma Etching: An Introduction, Academic Press, San Diego, CA, 1989.
[15] B. Chapman, Glow Discharge Processes, Wiley, New York, 1980.
[16] Ch. Steibruchel, Appl. Phys. Lett. 55 (1989) 1960.
[17] P. Singmund, in: Tolk (Ed.), Inelastic Ion-Surface Collisions, Academic, New York, 1977.
[18] D.J. Economou, R.C. Alkire, J. Electrochem. Soc. 135 (1988) 2786.
[19] J.P. Chang, J.C. Arnold, G.C.H. Zau, H.-S. Shin, H.H. Sawin, J. Vac. Sci. Technol. A 15 (1997) 1853.
[20] R.H. Bruce, in: R.G. Frieser, C.J. Mogab (Eds.), Plasma Processing, The Electrochemical Society, Pennington, NJ, 1981, p. 243.
[21] H.F. Winters, J. Vac. Sci. Technol. A 3 (1985) 786.
[22] J.F. Battey, J. Electrochem. Soc. 124 (1977) 437.
[23] D.J. Economou, R.C. Alkire, J. Electrochem. Soc. 132 (1985) 648.
[24] E. Meeks, R.S. Larson, S.R. Vosen, J.W. Shon, J. Electrochem. Soc. 144 (1997) 357.
[25] M.A. Lieberman, R.A. Gottscho, in: M. Francombe, J. Vossen (Eds.), Physics of Thin Films, Academic Press, San Diego, CA, 1993.
[26] J. Hopwood, Plasma Sources Sci. Technol. 1 (1992) 109.
[27] M. Meyyappan (Ed.), Computational Modeling in Semiconductor Processing Artech House, Boston, MA, 1994.
[28] L. Kline, M.J. Kushner, Crit. Rev. Solid State Mater. Sci. 16 (1989) 1.
[29] D.P. Lymberopoulos, D.J. Economou, J. Vac. Sci. Technol. A 12 (1994) 1229.
[30] E.S. Aydil, D.J. Economou, J. Electrochem. Soc. 140 (1993) 1471.
[31] D.P. Lymberopoulos, D.J. Economou, IEEE Trans. Plasma Sci. 23 (1995) 573.
[32] T.E. Nitschke, D.B. Graves, IEEE Trans. Plasma Sci. 23 (1995) 717.
[33] R.S. Wise, D.P. Lymberopoulos, D.I. Economou, Appl. Phys. Lett. 68 (1996) 2499.
[34] M. Meyyappan, T.R. Govindan, J. Appl. Phys. 78 (1995) 6432.
[35] M.J. Grapperhaus, M.J. Kushner, J. Appl. Phys. 81 (1997) 569.
[36] D.J. Economou, D. Evans, R.C. Akire, J. Electrochem. Soc. 135 (1988) 756.
[37] D.J. Economou, R.C. Alkire, J. Electrochem. Soc. 135 (1988) 941.
[38] M.K. Gobbert, T.P. Merchant, L.J. Borucki, T.S. Cale, J. Electrochem. Soc. 144 (1997) 3945.
[39] S.T. Rodgers, K.F. Jensen, J. Appl. Phys. 83 (1998) 524.
[40] C. Lee, D.B. Graves, M.A. Lieberman, D.W. Hess, J. Electrochem. Soc. 141 (1994) 1546.
[41] E. Meeks, J.W. Shon, IEEE Trans. Plasma Sci. 23 (1995) 539.
[42] S.C. Deshmukh, D.J. Economou, J. Appl. Phys. 72 (1992) 4597.
[43] V. Midha, D.J. Economou, Plasma Sources Sci. Technol. (submitted for publication).
[44] L.E. Kline, W.D. Partlow, W.E. Bies, J. Appl. Phys. 65 (1989) 70.
[45] I.C. Plump, K.R. Ryan, Plasma Chem. Plasma Process. 6 (1986) 205.
[46] M.J. Kushner, W.Z. Collison, M.J. Grapperhaus, J.P. Holland, M.S. Barnes, J. Appl. Phys. 80 (1996) 1337.
[47] M.J. Kushner, J. Appl. Phys. 82 (1997) 5312.
[48] M. Dalvie, K.F. Jensen, J. Vac. Sci. Technol. A 8 (1990) 1648.
[49] S.-K. Park, D.J. Economou, J. Electrochem. Soc. 137 (1990) 2624.
[50] E.S. Aydil, D.J. Economou, J. Electrochem. Soc. 139 (1992) 1396.
[51] D.B. Graves, K.F. Jensen, IEEE Trans. Plasma Sci. 14 (1986) 78.
[52] D.P. Lymberopoulos, D.J. Economou, J. Appl. Phys. 73 (1993) 3668.
[53] S.-K. Park, D.J. Economou, J. Appl. Phys. 68 (1990) 3904.
[54] A.D. Richards, B.E. Thompson, H.H. Sawin, Appl. Phys. Lett. 50 (1987) 492.
[55] M. Meyyappan, T.R. Govindan, J. Vac. Sci. Technol. A 10 (1992) 1344.
[56] G.R. Misium, A.M. Lichtenberg, M.A. Lieberman, J. Vac. Sci. Technol. A 7 (1989) 1007.
[57] N. Sato, H. Tagashira, IEEE Trans. Plasma Sci. 19 (1991) 102.
[58] T.J. Sommerer, M.J. Kushner, J. Appl. Phys. 71 (1991) 1654.
[59] M.H. Wilcoxson, V.1. Manousiouthakis, J. Comp. Phys. 115 (1994) 376.
[60] D.P. Lymberopoulos, D.J. Economou, Appl. Phys. Lett. 63 (1993) 2478.
[61] P.L.G. Ventzek, T.J. Sommerer, R.J. Hoekstra, M.J. Kushner, Appl. Phys. Lett. 62 (1993) 3247.
[62] D.P. Lymberopoulos, D.J. Economou, J. Res. Natl. Inst. Stand. Technol. 100 (1995) 473.

[63] J.D. Bukowski, D.B. Graves, J. Appl. Phys. 80 (1996) 2614.
[64] P.L.G. Ventzek, R.J. Hoekstra, M.J. Kushner, J. Vac. Sci. Technol. B 12 (1994) 461.
[65] M. Dalvie, M. Surendra, G.S. Selwyn, Appl. Phys. Lett. 62 (1993) 3207.
[66] F.F. Young, C.-H. Wu, IEEE Trans. Plasma Sci. 21 (1993) 312.
[67] J.D.P. Passchier, W.J. Goedheer, J. Appl. Phys. 74 (1993) 3744.
[68] J.P. Bouef, L.C. Pitchford, Phys. Rev. E 51 (1995) 1376.
[69] M.H. Wilcoxson, V.1. Manousiouthakis, Chem. Eng. Sci. 51 (1996) 1089.
[70] D.J. Economou, J. Feldsien, R.S. Wise, in: U. Kortshagen, L.D. Tsendin (Eds.), Electron Kinetics and Applications, Plenum Press, New York, 1998.
[71] E. Gogolides, H.H. Sawin, J. Appl. Phys. 72 (1992) 3971.
[72] R.P. Brinkman, R.F. Furst, C. Werner, M. Hierlemann, in: M. Meyyappan, D.J. Economou, S.W. Butler (Eds.), Proc. 1st Int. Symp. Control, Diagnostics and Modeling in Semiconductor Manufacturing, The Electrochemical Society, Pennington, NJ, 1995.
[73] D.J. Economou, R.S. Wise, D.P. Lymberopoulos, in: G. Mathad, M. Meyyappan (Eds.), Plasma Processing XI, Vol. 96–12, The Electrochemical Society, Pennington, NJ, 1996.
[74] J. Feldsien, D.J. Economou, Thin Solid Films, to be submitted.
[75] M. Surendra, Plasma Sources Sci. Technol. 4 (1995) 56.
[76] C.K. Birdsall, IEEE Trans. Plasma Sci. 19 (1991) 65.
[77] V. Vahedi, G. DiPeso, C.K. Birdsall, M.A. Lieberman, T.D. Ronglien, Plasma Sources Sci. Technol. 2 (1993) 261.
[78] D.J. Economou, T.J. Bartel, R.S. Wise, D.P. Lymberopoulos, IEEE Trans. Plasma Sci. 23 (1995) 581.
[79] M.D. Kilgore, H.M. Wu, D.B. Graves, J. Vac. Sci. Technol. B 12 (1994) 494.
[80] V. Serikov, K. Nanbu, J. Vac, Sci. Technol. A 14 (1996) 3108.
[81] D.P. Lymberopoulos, D.J. Economou, J. Phys. D: Appl. Phys. 28 (1995) 727.
[82] H.R. Skullerud, J. Phys. D: Appl. Phys. 1 (1968) 1567.
[83] U. Kortshagen, I. Pukropski, L.D. Tsendin, Phys. Rev. E 51 (1995) 6063.
[84] V.I. Kolobov, V.A. Godyak, IEEE Trans. Plasma Sci. 23 (1995) 503.
[85] S. Samukawa, T. Mieno, Plasma Sources Sci. Technol. 5 (1996) 132.
[86] T.H. Ahn, N. Nakamura, H. Sugal, Plasma Sources Sci. Technol. 5 (1996) 139.
[87] W.B. Pennebaker, IBM J. Res. Dev. 23 (1979) 16.
[88] R.T. Farouki, M. Dalvie, L.F. Pavarino, J. Appl. Phys. 68 (1990) 6106.
[89] K.-U. Riemann, Phys. Fluids 24 (1981) 2163.
[90] C.A. Ordonez, Phys. Fluids B 4 (1992) 778.
[91] V.A. Godyak, N. Sternberg, Phys. Rev. A 42 (1990) 2299.
[92] A. Metze, D.W. Ernie, H.J. Oskam, J. Appl. Phys. 60 (1986) 3081.
[93] M.A. Lieberman, IEEE Trans. Plasma Sci. 17 (1989) 338.
[94] W.J. Goedheer, P.M. Meijer, IEEE Trans. Plasma Sci. 19 (1991) 245.
[95] R.T. Farouki, S. Hamaguchi, M. Dalvie, Phys. Rev. A 45 (1992) 5913.
[96] M.J. Kushner, J. Appl. Phys. 58 (1985) 4024.
[97] M.S. Barnes, J.C. Foster, J.H. Keller, IEEE Trans. Plasma Sci. 19 (1991) 240.
[98] P. Benoit-Cattin, L.C. Bernard, J. Appl. Phys. 39 (1968) 5273.
[99] P.A. Miller, M.E. Riley, J. Appl. Phys. 82 (1997) 3689.
[100] T. Panagopoulos, D.J. Economou, J. Appl. Phys 85 (1999) 3435.
[101] R.A. Gottscho, C.W. Jurgensen, D.J. Vitkavage, J. Vac. Sci. Technol. B 10 (1992) 2133.
[102] E.S. Shaqfeh, C.W. Jurgensen, J. Appl. Phys. 66 (1989) 4664.
[103] N.R. Rueger, J.J. Beulens, M. Schaepkens, M.F. Doemling, J.M. Mirza, T.E.F.M. Standaert, G.S. Oehrlein, J. Vac, Sci. Technol. A 15 (1997) 1881.
[104] J.W. Coburn, H.F. Winters, J. Vac. Sci. Technol. 16 (1979) 391.
[105] M. Sato, Y. Arita, J. Vac. Sci. Technol. B 16 (1998) 1038.
[106] T. Nozawa, T. Kinoshita, T. Nishizawa, A. Narai, T. Inoue, A. Nakaue, Jpn. J. Appl. Phys. 34 (1995) 2107.
[107] T. Kinoshita, M. Hane, J.P. McVittie, J. Vac. Sci. Technol. B 14 (1996) 560.
[108] G.S. Hwang, K.P. Giapis, J. Vac. Sci. Technol. B 15 (1997) 70.
[109] H. Ootera, T. Oomori, M. Tuda, K. Namba, Jpn. J. Appl. Phys. 33 (1994) 4276.
[110] E.W. Scheckler, A.R. Neureuther, IEEE Trans. Computer-Aided Design 13 (1994) 219.
[111] S. Hamaguchi, M. Dalvie, R.T. Farouki, S. Sethuraman, J. Appl. Phys. 74 (1993) 5172.
[112] D.G. Coronell, K.F. Jensen, J. Computer-Aided, Mater. Design 1 (1993) 3.
[113] J.A. Levinson, E.S.G. Shaqfeh, J. Vac. Sci. Technol. A (1997) 15.
[114] R.J. Hoekstra, M.J. Grapperhaus, M.J. Kushner, J. Vac. Sci. Technol. A (1997) 15.
[115] M. Mazhar Islam Raja, M.A. Capelli, J.P. McVittie, K.C. Saraswat, J. Appl. Phys. 70 (1991) 7137.
[116] T.S. Cale, V. Mahadev, in: S. Rossnagel, A. Ulman (Eds.), Modeling of Film Deposition for Microelectronic Applications, Thin Films, Vol. 22, Academic Press, New York, 1996, p. 175.
[117] T.S. Cale, G.B. Raup, T.H. Gandy, J. Vac. Sci. Technol. A 10 (1992) 1128.
[118] V.K. Singh, E.S.G. Shaqfeh, J.P. McVittie, J. Vac. Sci. Technol. B 10 (1992) 1091.
[119] S. Hamaguchi, M. Dalvie, J. Electrochem. Soc. 141 (1994) 1964.
[120] H.F. Schaefer III (Ed.), Modern Theoretical Chemistry, Vols. 3 and 4, Plenum Press, New York, 1977.
[121] M.C. Payne, M.P. Teter, D.C. Allan, T.A. Arias, J.D. Joannopoulos, Rev. Mod. Phys. 64 (1992) 1045.
[122] J.M. Haile, Molecular Dynamics Simulation: Elementary Methods, Wiley, New York, 1992.
[123] M.P. Allen, D.J. Tildesley, Computer Simulation of Liquids, Oxford University Press, Oxford, 1990.
[124] M.H. Kalos, P.A. Witlock, Monte Carlo Methods. Part I: Theory, Wiley, New York, 1986.
[125] H.H. Andersen, Nucl. Instrum. Methods Phys. Res. B 18 (1987) 321.
[126] K.H. Muller, Phys. Rev. B 35 (1987) 7906.
[127] T.A. Schoolcraft, B.J. Garrison, J. Am. Chem. Soc. 113 (1991) 8221.
[128] H. Feil, J. Dieleman, B.J. Garrison, J. Appl. Phys. 74 (1993) 1303.
[129] M.E. Barone, D.B. Graves, J. Appl. Phys. 77 (1995) 1263.
[130] S. Athavale, D.J. Economou, J. Vac. Sci. Technol. A 13 (1995) 966.
[131] N.A. Kubota, D.J. Economou, S. Plimpton, J. Appl. Phys. 83 (1998) 4055.
[132] N.A. Kubota, Ph.D. Dissertation, University of Houston, 1998.
[133] N. Layadi, V.M. Donnelly, J.T.C. Lee, F.P. Klemens, J. Vac. Sci. Technol. A 15 (1997) 604.
[134] S. Das Sarma, J. Vac. Sci. Technol. A 8 (1990) 2714.
[135] C.C. Battaile, D.J. Srolovitz, J.E. Butler, J. Appl. Phys. 82 (1997) 6293.
[136] NRC, Plasma Processing of Materials: Scientific Opportunities and Technological Challenges: NRC Report, National Academy, Washington, DC, 1991.
[137] O. Auciello, D.L. Flamm (Eds.), Plasma Diagnostics, Vols. 1 and 2 Academic, San Diego, CA, 1989.
[138] J.D. Swift, M.J.R. Schwar, Electrical Probes for Plasma Diagnostics, Elsevier, New York, NY, 1969.
[139] F.F. Chen, in: R.H. Huddlestone, S.L. Leonard (Eds.), Plasma Diagnostics, Academic, New York, 1965.
[140] B.E. Cherrington, Plasma Chem. Plasma Process. 2 (1982) 113.
[141] T.F. Kuech, P.D. Dapkus, Y. Aoyagi (Eds.), Atomic Layer Growth and Processing, MRS Symp. Proc., MRS, Pittsburgh, PA, Vol. 222, 1991.